

1 **Title**

2 Quorum sensing and stress-activated MAPK signaling repress yeast to hypha transition in the fission
3 yeast *Schizosaccharomyces japonicus*.

4

5 **Short Title**

6 Quorum sensing in the fission yeast *Schizosaccharomyces japonicus*.

7

8

9 **Author list**

10 Elisa Gómez-Gil¹, Alejandro Franco¹, Marisa Madrid¹, Beatriz Vázquez-Marín¹, Mariano Gacto¹, Jesualdo
11 Fernández-Breis², Jero Vicente-Soler¹, Teresa Soto^{1#} and José Cansado^{1#}.

12 ¹Yeast Physiology Group, Departamento de Genética y Microbiología, Facultad de Biología. Universidad de
13 Murcia. 30071 Murcia, Spain.

14 ²Departamento de Informática y Sistemas, Facultad de Informática. Universidad de Murcia. 30071 Murcia,
15 Spain.

16

17

18 [#]Corresponding authors:

19 José Cansado, Department of Genetics and Microbiology, Universidad de Murcia, 30071 Murcia, Spain.

20 e-mail: jcansado@um.es

21 Teresa Soto, Department of Genetics and Microbiology, Universidad de Murcia, 30071 Murcia, Spain.

22 e-mail: teresaso@um.es

23

24

25

26 **Abstract**

27 Quorum sensing (QS), a mechanism of microbial communication dependent on cell density, governs
28 developmental decisions in many bacteria and in some pathogenic and non-pathogenic fungi including yeasts.
29 In these simple eukaryotes this response is mediated by the release into the growth medium of quorum-
30 sensing molecules (QSMs) whose concentration increases proportionally to the population density. To date
31 the occurrence of QS is restricted to a few yeast species. We show that a QS mediated by the aromatic
32 alcohols phenylethanol and tryptophol represses the dimorphic yeast to hypha differentiation in the fission
33 yeast *S. japonicus* in response to an increased population density. In addition, the stress activated MAPK
34 pathway (SAPK), which controls cell cycle progression and adaptation to environmental changes in this
35 organism, constitutively represses yeast to hypha differentiation both at transcriptional and post-translational
36 levels. Moreover, deletion of its main effectors Sty1 MAPK and Atf1 transcription factor partially suppressed
37 the QS-dependent block of hyphal development under inducing conditions. RNAseq analysis showed that the
38 expression of *nrg1*⁺, which encodes a putative ortholog of the transcription factor Nrg1 that represses yeast to
39 hypha dimorphism in *C. albicans*, is downregulated both by QS and the SAPK pathway. Remarkably, Nrg1
40 may act in *S. japonicus* as an activator of hyphal differentiation instead of being a repressor. *S. japonicus*
41 emerges as an attractive and amenable model organism to explore the QS mechanisms that regulate cellular
42 differentiation in fungi.

43

44 **Author Summary**

45 Quorum sensing is a relevant mechanism of communication dependent on population density that controls cell
46 development and pathogenesis in microorganisms including fungi. We describe a quorum sensing mediated
47 by the release of aromatic alcohols in the growth medium that blocks hyphal development in the fission yeast
48 *Schizosaccharomyces japonicus*. This is the first description of such a mechanism in the fission yeast lineage,
49 and confirms its expansion along Ascomycota fungi. The stress-responsive pathway (SAPK), which regulates
50 fungal growth and differentiation, limits hyphal growth in *S. japonicus* in a constitutive fashion, and
51 nonfunctional SAPK mutants are partially insensitive to quorum sensing and able to form hyphae in high cell
52 density cultures. Nrg1, an important factor that blocks hyphal development in the pathogen *Candida albicans*,
53 activates hyphal growth in *S. japonicus*, and its expression counteracted by both quorum sensing and the
54 SAPK pathway. Nrg1 function may thus have diverged evolutionary in this organism from being a repressor
55 to an activator of hyphal development. *S. japonicus* emerges as a suitable model organism to explore the
56 intricate mechanisms regulating fungal differentiation.

57

58 **Introduction**

59 The highly conserved mitogen-activated protein kinase (MAPK) signaling pathways are key players
60 in eukaryotic cells to elicit proper adaptive responses to environmental changes. Once activated in response to
61 external and internal cues, MAPKs phosphorylate a wide range of extranuclear proteins and/or shift into the
62 nucleus to phosphorylate transcription factors that do, in turn, execute transcriptional programs that promote
63 cellular adaptation to the triggering stimulus [1]. The stress-activated pathway (SAPK), one of the three
64 MAPK pathways present in the rod-shaped fission yeast *Schizosaccharomyces pombe*, shows significant
65 functional homology to the mammalian p38 pathway [2], and plays a critical role in the control of cell cycle
66 and the general response to stress. Its central element, the MAPK Sty1, becomes phosphorylated at two
67 conserved threonine and tyrosine residues within its activation loop in response to multiple stressful
68 conditions [2]. Activated Sty1 then moves in turn to the nucleus and phosphorylates the bZIP domain
69 transcription factor Atf1 to modulate the expression of a group of genes including the CESR (Core
70 Environmental Stress Response) genes, which participate in the consequent adaptive cell response. Activated
71 Sty1 also controls mRNA stabilization, cell cycle progression at the G2/M transition, and polarized growth
72 during growth and stress [2, 3].

73 The fission yeast species *S. japonicus* is becoming an attractive model organism to explore
74 evolutionary physiological and developmental changes within the *Schizosaccharomyces* clade [4, 5].
75 However, the biological significance of the stress-activated MAP kinase signaling pathway in *S. japonicus*
76 remains to be established. Both *S. pombe* and *S. japonicus* grow by binary fission during vegetative growth
77 and share similar mechanisms for conjugation and sporulation. However, *S. japonicus* has distinctive features
78 including a defective respiration, a highly dynamic actin cytoskeleton, and semi-open mitosis [6-12]. *S. pombe*
79 and *S. japonicus* are able to show pseudohyphal/hyphal growth under specific conditions, although the
80 penetrance of such phenotype is very different in the two species. Pseudohyphal growth in *S. pombe* requires
81 high cell density and occurs in strains of specific genetic backgrounds growing in media with low nitrogen
82 content and abundant carbon source [13-15]. In contrast, *S. japonicus* cells undergo robust yeast to hypha
83 differentiation in either liquid or solid media under various conditions including nutrient stress [16-19], or
84 DNA damage induced with camptothecin (CPT), a topoisomerase I inhibitor [19, 20]. Indeed, low CPT

85 concentrations trigger yeast to hypha transition through a mechanism involving the Chk1 kinase and the
86 Rad3–Rad9 pathway, but without induction of checkpoint arrest [20, 21]. Moreover, differentiation is a
87 reversible process, and hyphal cells quickly return to the fission yeast morphology after drug removal from the
88 growth medium [20]. This feature makes *S. japonicus* a suitable model organism to unveil novel and crucial
89 mechanisms for the comprehension of the dimorphism process.

90 Quorum sensing (QS) is a mechanism of microbial communication dependent on cell density that
91 governs developmental decisions in many bacterial species and in some pathogenic and non-pathogenic yeast
92 species like *Candida albicans* and *Saccharomyces cerevisiae* [22-24]. The main effectors of QS, known as
93 auto-inducers or quorum-sensing molecules (QSM), are secreted into the growth medium and their
94 concentration increases proportionally to the population density [22, 23]. Fungal QSMs, which include acyclic
95 and/or aromatic alcohols such as farnesol, tyrosol, phenylethanol and tryptophol, impact morphogenesis,
96 germination of macroconidia and apoptosis [22, 23]. Consequently, they also play a role in fungal
97 pathogenesis, as is the case with farnesol and tyrosol, which modulate yeast to hyphae morphological switch
98 and biofilm formation in *C. albicans* [22, 23].

99 In this work we demonstrate the existence of an inducible cell density dependent QS in *S. japonicus*
100 that negatively controls yeast to hypha transition and that is mediated by aromatic alcohols. This mechanism is
101 reinforced by the SAPK pathway, which also negatively regulates hyphal initiation and maintenance in a
102 constitutive fashion. Remarkably, QS and the Sty1-Atf1 pathway downregulate the expression of Nrg1,
103 which, contrary to its *C. albicans* ortholog [25, 26], is not a repressor but an activator of hyphal
104 differentiation.

105

106 **Results**

107 **A quorum sensing mechanism mediated by aromatic alcohols inhibits yeast to hypha transition in *S.*** 108 ***japonicus*.**

109 Treatment of exponentially growing wild type *S. japonicus* yeast cells with very low doses of CPT
110 (0.2 μ M) prompts their differentiation into filamentous cells (hyphae) with relative quick kinetics and without
111 inducing a checkpoint arrest [20]. We noticed that the ability of *S. japonicus* yeast cells to differentiate into

112 filaments and/or hyphae inversely correlates with the initial population density present in the medium. In our
113 experimental setup the average cell length of filamentous wild type cells after 6h of incubation in the presence
114 of 0.2 μM CPT ($\sim 40 \mu\text{m}$) did not changed significantly when the initial inoculum was of $5.5 \cdot 10^5$ or 10^6
115 cells/ml (Fig 1A). However, cell differentiation became strongly limited when cells where inoculated at \geq
116 $2 \cdot 10^6$ cells/ml ($\sim 18 \mu\text{m}$), and progressively reduced as cell density was raised to 10^7 cells/ml ($\sim 10 \mu\text{m}$) (Fig
117 1A). *S. japonicus* cells divided normally during the course of the experiment at these population densities (Fig
118 1A), confirming that inhibition of the dimorphic switch was not due to a growth arrest. Therefore, a quorum
119 sensing mechanism might be responsible for the inhibition of hyphal differentiation of *S. japonicus* at high
120 cell densities. As support for this hypothesis, the elongated/hyphal cells induced with CPT where almost
121 undetectable when the wild type strain was inoculated at a low density (10^6 cells/ml) in filter-sterilized
122 conditioned medium obtained from a high cell density culture of the same strain ($>5 \cdot 10^7$ cells/ml) (Fig 1B).
123 Contrariwise, filamentation in the presence of CPT was very strong when the wild type strain was inoculated
124 at low density in unconditioned medium supplemented with the same glucose concentration ($\sim 3\%$) remaining
125 in the conditioned medium (Fig 1B). Accordingly, the average cell length of CPT-treated wild type cells
126 incubated for 6h in unconditioned medium became progressively reduced when incubated in conditioned
127 medium obtained from $5 \cdot 10^6$, $5 \cdot 10^7$, and 10^8 cells/ml density cultures ($43.8 \pm 14,6 \mu\text{m}$ versus $21.6 \pm 11,6$,
128 14.4 ± 5.5 and $11.4 \pm 1.9 \mu\text{m}$, respectively; Fig 1C). *S. japonicus* strains produce a readily visible mycelium
129 when cultured for several days in a malt extract-based solid medium (YEMA) [19]. This provides an
130 alternative biological readout to CPT treatment to explore a putative negative role of QS during hyphal growth
131 progression in response to nutritional changes. As compared to unconditioned medium, the mycelial area
132 expansion of wild type cells in YEMA plates also decreased progresively when supplemented with
133 conditioned medium obtained from $5 \cdot 10^6$ cells/ml $5 \cdot 10^7$ cells/ml density cultures (Fig 1D).

134 Several acyclic and/or aromatic alcohols, such as farnesol, tyrosol, phenylethanol and tryptophol have
135 been described to mediate QS in yeasts species from the genera *Candida*, *Debaryomyces* and *Saccharomyces*
136 [22, 23]. To identify the QS molecule/s responsible for the inhibition of *S. japonicus* hyphal growth at high
137 population densities, the conditioned medium obtained from a stationary phase culture was extracted with
138 organic solvents, and the lipophilic compounds were separated, identified, and quantified by GC/MS,
139 HPLC/MS and/or HPLC/UV analysis. This experimental approach, which included a comparative analysis of

140 chemically synthesized standards, revealed the presence of different peaks that were unequivocally identified
141 as phenylethanol, tyrosol, and tryptophol (Fig S1 and Materials and Methods). The accumulation of these
142 aromatic alcohols in the culture medium was growth phase-dependent, and reached a maximum during
143 stationary phase (~100 μ M for phenylethanol, ~75 μ M for tyrosol, and ~10 μ M for tryptophol; Fig 1E). We
144 found that the cell length average of CPT-treated wild type cells after 6h of incubation in rich medium at low
145 population density (initial inoculum of 10^6 cells/ml) became significantly reduced in the presence of 1 mM
146 phenylethanol and/or tryptophol, but not with tyrosol (Fig 1F). Furthermore, the growth of *S. japonicus* wild
147 type cells was not altered in the presence of ≤ 2 mM of the above aromatic alcohols in the growth medium
148 (Fig S2). As compared to untreated medium, the mycelial area expansion of wild type cells in YEMA plates
149 was significantly decreased in the presence of 1 mM of either phenylethanol or tryptophol, and further
150 reduced with a combination of both alcohols (Fig 1G). Contrariwise, mycelium expansion was not negatively
151 affected by the addition of tyrosol (Fig 1G). Virtually identical results were obtained after incubation in YES
152 solid media plates supplemented with 10% red grape extract (RGE medium), which has been recently shown
153 to induce strong a mycelial development in *S. japonicus* (Fig 1G) [27]. Altogether, these results demonstrate
154 the existence of a QS mechanism mediated by the aromatic alcohols phenylethanol and tryptophol in *S.*
155 *japonicus* that represses dimorphic yeast to hypha differentiation in response to increased population density.

156

157 **The stress-responsive functions of the SAPK pathway are conserved in *S. japonicus***

158 Sty1, the key member of the SAPK pathway, controls multiple cellular events in response to
159 environmental cues in *S. pombe* [2]. An amino-acid sequence comparison (ClustalW) revealed that the
160 putative MAPK Sty1 in *S. japonicus* (Gene ID: SJAG_02592) shows ~94% identity with *S. pombe* Sty1 (Fig.
161 S3). This includes residues involved in ATP binding, the proton acceptor site, MAPKK (-DXXD- motif) and
162 common (-ED- motif) docking sites, as well as the -TGY- activation loop present in MAP kinases of the p38
163 type (Fig. S3) [28]. By employing anti-Hog1 and phospho-p38 antibodies that specifically detect the
164 respective total and dually phosphorylated isoforms in yeast MAPKs of the p38 type [29], a single band of the
165 predicted molecular weight (~42 kDa) was detected with both antibodies in extracts from exponentially
166 growing *S. japonicus* wild type cells (Fig. S3). These signals were totally absent in extracts from a *S.*

167 *japonicus* strain lacking the putative Sty1 ORF via homologous recombination (*sty1*Δ; see Materials and
168 Methods; Fig. S3), thereby confirming that it encodes the sole p38-type MAPK present in this organism.

169 In *S. pombe* Sty1 positively regulates cell cycle progression during the G2/M transition, the initiation
170 of sexual differentiation and the chronological lifespan [30-32]. *S. japonicus sty1*Δ cells also display elongated
171 cell length at division as compared to control cells (25.5 ± 2.5 vs 18.8 ± 1.8 μm; Fig 2A) , and either h⁺ or h⁻
172 heterotallic kinase-deleted mutants were totally defective for mating when crossed with wild type cells of the
173 opposite mating types (Fig 2B). In addition, *S. japonicus sty1*Δ cells quickly lost viability in stationary phase
174 cultures after 2-3 days of growth in rich medium as measured by either phloxine B staining or growth plate
175 assays (Fig S4). The relative total levels of Sty1 in unperturbed exponentially growing *S. japonicus* cells were
176 approximately half of those present in *S. pombe*. However, basal Sty1 phosphorylation in *S. japonicus* was
177 significantly increased as compared to that of *S. pombe* (Fig 2C), and maintained relatively constant during
178 the growth curve at cellular densities ranging from $2 \cdot 10^6$ to $2 \cdot 10^8$ cells/ml (Fig S3). The specific tyrosine
179 phosphatase Pyp1 is the main negative regulator of basal Sty1 phosphorylation in *S. pombe* [2]. Similar to the
180 equivalent *S. pombe* mutant, *S. japonicus* cells with a deletion in the Pyp1 ortholog (gene ID SJAG_02013)
181 displayed a clear reduction in cell length at division as compared to the wild type strain (11.0 ± 0.2 μm; Fig
182 2A). Hence, the role of Pyp1 as a negative regulator of Sty1 function may be conserved in both fission yeast
183 species. *S. pombe* Sty1 is activated in response to multiple stress conditions such as heat shock, saline, or
184 oxidative stress, as well as and glucose deprivation, in order to promote cellular adaptation to environmental
185 changes (Fig 2D) [2, 33]. Similarly, *S. japonicus* Sty1 became highly activated when cultures were incubated
186 at 45°C (heat shock), treated with 0.6 M KCl (salt stress), after addition of 0.5 mM hydrogen peroxide
187 (oxidative stress), or starved from glucose (Fig 2D). The growth sensitivity of *S. pombe sty1*Δ cells in
188 response to high temperature, saline stress (KCl), oxidative stress (hydrogen peroxide), caffeine and SDS [2,
189 33, 34], was also shared by the *S. japonicus sty1*Δ mutant (Fig 2E). The bZIP domain protein Atf1 is the main
190 transcription factor regulated downstream by Sty1 in *S. pombe* [35]. A Blast search revealed the presence of a
191 single Atf1 ortholog in *S. japonicus* genome (Gene ID: [SJAG_00266](#)). *S. japonicus* Atf1 shows an overall
192 ~43.5% amino acid identity with *S. pombe* Atf1 (Fig. S3). The HRA, osmotic stress, and basic-leucine zipper
193 domains involved in recombination, stress response, and DNA binding, respectively [36], are strongly
194 conserved in *S. japonicus* Atf1 with regard to the *S. pombe* counterpart (88, 61.3, and 95.3% identity,

195 respectively), and also includes several of the putative MAPK-dependent phosphorylation sites (SP/TP) present
196 in *S. pombe* Atf1 (Fig. S3). Remarkably, a *S. japonicus* mutant lacking the Atf1 ortholog (*atf1Δ* strain) showed
197 a defective G2/M progression similar to that of the *sty1Δ* mutant (cell length at division: $24.3 \pm 4.5 \mu\text{m}$; Fig
198 2A). As compared to *sty1Δ* cells, *S. japonicus atf1Δ* cells were slightly less defective during mating (Fig 2B),
199 and showed a significant growth sensitivity in response to stress (Fig. 2E). The above results indicate that the
200 SAPK pathway plays a critical role in the regulation of cell cycle progression, the sexual differentiation, the
201 chronological lifespan, and the general cellular adaptive response to environmental stress in *S. japonicus*.
202 They also suggest that many of these functions may rely on the transcriptional activity mediated by Atf1.

203

204 **SAPK function negatively modulates induction and progression of hyphal growth in *S. japonicus*.**

205 When growing in solid rich medium (YES-agar; 24h) *S. japonicus sty1Δ* and *atf1Δ* mutants displayed
206 a wash-resistant invasive phenotype that is absent in wild type and *pyp1Δ* cells (Fig 3A), suggesting the
207 existence of an altered developmental and/or growth pattern. *S. japonicus* morphological transition from yeast
208 to hypha during inducing conditions (i.e. after CPT treatment or in RGE medium) involves three successive
209 stages that are known as vacuolated yeast (bipolar growing cells with and numerous cytoplasmic vacuoles),
210 transition forms (monopolar growing cells with and numerous small vacuoles at the non-growing end), and
211 hyphae (large monopolar growing cells with 1-2 large vacuoles at the non-growing end) [16, 27]. Remarkably,
212 as compared to wild type cells, both SAPK mutants, and in particular the *sty1Δ* mutant, showed a significant
213 increase in the number of vacuolated yeast, transition forms and/or hyphae after 12 hours of growth under
214 non-inducing conditions rich YES-agar plates (Fig 3B). The average cell length of filamentous *sty1Δ* and
215 *atf1Δ* cells after 6h of incubation in rich medium supplemented with $0.2 \mu\text{M}$ CPT was significantly higher
216 than in wild type cells ($81,5 \pm 15,4 \mu\text{m}$ and $67,3 \pm 16,6 \mu\text{m}$ in *sty1Δ* and *atf1Δ* cells *versus* $42,6 \pm 16 \mu\text{m}$ in
217 wild type cells; Fig. 3C), whereas differentiation in *pyp1Δ* cells became strongly impaired ($13,9 \pm 3,6 \mu\text{m}$; Fig.
218 3C). Wild type, *sty1Δ*, *atf1Δ*, and *pyp1Δ* mutants grew normally at those CPT concentrations (Fig S4).
219 Moreover, total and activated Sty1 levels remained unchanged and irrespective of the presence or absence of
220 CPT in the medium (Fig 3D). Thus, in *S. japonicus* the SAPK pathway appears to negatively impact the
221 induction of hyphal differentiation in a constitutive fashion. Prolonged incubation in the presence of CPT
222 (24h) produced a much higher percentage of filaments and/or hypha in *sty1Δ* and *atf1Δ* mutants than in wild

223 type cells (~98% and ~75% versus ~12%, respectively), while they remained absent in *pyp1Δ* cells (Fig 3E).
224 Interestingly, *sty1Δ* hyphae were highly branched as compared to those from the *atf1Δ* mutant (~50% versus
225 ~10%, respectively) (Fig 3E), suggesting that Sty1 function, but not Atf1, negatively affects the later stages of
226 hyphal differentiation. Congruent with the above prediction, the *sty1Δ* mutant showed a significant increase in
227 the mycelial area of expansion with respect to either wild type or *atf1Δ* cells when incubated in YEMA plates
228 (Fig 3F). Contrariwise, mycelium production under the above conditions was strongly reduced in *pyp1Δ* cells
229 (Fig 3F). Hence, in *S. japonicus* the SAPK pathway effectors Sty1 MAPK and Atf1 transcription factor
230 downregulate the initiation of yeast to hypha transition in response to environmental cues, and Sty1
231 additionally represses the later stages of hyphal differentiation in an Atf1-independent fashion. Moreover, our
232 results indicate that Sty1 phosphorylation must be maintained under a certain threshold to allow efficient yeast
233 to hypha differentiation, and suggest that an increase in MAPK activity may result in a complete inhibition of
234 this process. Indeed, treatment of low density *S. japonicus* cultures with either 0.3 M or 0.6M KCl that
235 hyperactivate Sty1 (Fig 2D), reduced hyphal differentiation in the presence of CPT (Fig 3G), and mycelial
236 expansion in YEMA plates, respectively (Fig 3H).

237

238 ***S. japonicus* QS is attenuated in the absence of SAPK function.**

239 The observation that a QS mechanism and the SAPK pathway negatively regulate the induction and
240 progression of *S. japonicus* hyphal growth prompted us to analyze the possible functional relationship
241 between both pathways. We found that *sty1Δ* and, to a lesser extent, *atf1Δ* cells were able to differentiate into
242 filaments to some extent after 6h of incubation in the presence of 0.2 μM CPT when inoculated at an initial
243 cell density of $5 \cdot 10^6$ cells/ml that completely blocks hyphal differentiation in wild type cells (Fig 4A). This
244 behavior was observed in the *sty1Δ* mutant even at higher densities of $5 \cdot 10^7$ cells/ml (Fig 4A). The ability of
245 *sty1Δ* and *atf1Δ* mutants to partially suppress cell density dependent inhibition of hyphal differentiation was
246 not due to a defective production of QSMs, since the levels of phenylethanol and tryptophol in the respective
247 cultures were similar to those of wild type cells (Fig 4B). Moreover, and in agreement with the above results,
248 CPT-treated *sty1Δ* and *atf1Δ* mutants were able to partially differentiate into elongated forms when incubated
249 in conditioned medium obtained from $5 \cdot 10^7$ and 10^8 cells/ml density cultures, which strongly inhibits the

250 morphological transition in wild type cells (Fig 4C). Finally, exogenous addition of increased concentrations
251 of QSMs (phenylethanol from 1 to 10 mM; 60 min) did not change basal Sty1 phosphorylation status in
252 exponentially growing *S. japonicus* cultures (Fig 4D). Altogether, these observations further confirm the
253 biological relevance in *S. japonicus* of the SAPK pathway as a constitutive repressor of hyphal development
254 that allows QS to operate over a specific cell density threshold.

255

256 **Nrg1 is an activator of hyphal growth in *S. japonicus* whose basal and induced expression is repressed**
257 **by the SAPK pathway and QS.**

258 Our findings suggest that the SAPK pathway through the Sty1–Atf1 branch may act transcriptionally
259 to repress hyphal initiation in *S. japonicus*. To obtain further insight into this hypothesis, we performed a
260 transcriptome analysis via high-coverage RNA sequencing (RNAseq). We thereby specifically searched for
261 differentially expressed genes in *sty1Δ* and *atf1Δ* mutants up- and down-regulated as compared to wild type
262 cells, and whose products might positively or negatively regulate yeast to hypha dimorphic switch. Two
263 biological replicates were tested for global gene expression in wild type *versus sty1Δ* and *atf1Δ* strains
264 growing in rich medium at the early exponential growth phase. As shown in Fig 5A, transcript levels of 29
265 genes from a total of 188 (~15%) were increased more than twofold (\log_2 fold change ≥ 1) in both *sty1Δ* and
266 *atf1Δ* mutants as compared to wild type cells, whereas 37 genes from a total of 171 (~22%) were
267 downregulated (\log_2 fold change ≤ -1) in both mutants. Contrariwise, only 5 (~3%) and 14 (~5%) genes were
268 up- and downregulated, or down- and upregulated, respectively, in both *sty1Δ* and *atf1Δ* mutants. Hence, while
269 there is a relatively low level of similarity in gene expression changes between *sty1Δ* and *atf1Δ* cells during
270 unperturbed growth, shared induction or repression of common genes is enriched in both mutants. A heatmap
271 of the subset of common up- and downregulated genes revealed evident differences in expression between
272 *sty1Δ* and *atf1Δ* mutants (Fig 5B). The complete gene lists of specific and common up- and downregulated
273 genes is shown in Table S3. Validation of RNAseq data was made through qPCR, for which a set of six
274 significantly differentially expressed genes up- and downregulated in *sty1Δ* and *atf1Δ* mutants as compared to
275 wild type cells was confirmed (Fig S5). Approximately half of the identified common up-regulated genes
276 encode putative hypothetical proteins without assigned function (Tables S1 to S8). The remaining 15 genes

277 were functionally categorized by gene ontology (GO) terms and include, among others, urea, glucose, and
278 amino acids plasma membrane transporters, as well as others involved in the oxidation-reduction process (Fig
279 S6). Similarly, half of the common down-regulated genes encode either fungal and/or hypothetical proteins
280 without assigned function whereas the other 23 are functionally diverse, including genes involved in
281 oxidation-reduction mechanisms, cell wall ascospore formation, DNA metabolism, and transcription (Fig S6).

282 Among the genes whose mRNA expression is induced in both *sty1Δ* and *atf1Δ* mutants we identified
283 *nrg1⁺*, which encodes a putative ortholog of the C₂H₂ zinc finger transcriptional repressor Nrg1 that negatively
284 regulates, respectively, pseudohyphal growth and yeast to hypha dimorphism in *S. cerevisiae* and *C. albicans*
285 [25, 26, 37]. *S. japonicus* Nrg1 is a putative 217 amino-acids protein with a low level of overall sequence
286 identity with *C. albicans* Nrg1 (~27%), that rises to ~57% within the 50 amino-acids C₂H₂ zinc finger region
287 (Fig. S7). qPCR analysis confirmed that *nrg1⁺* mRNA levels increase ~3 to ~7 fold in exponentially growing
288 *sty1Δ* and *atf1Δ* mutants, respectively, as compared to wild type cells (Fig 5C). Contrariwise, *nrg1⁺* mRNA
289 levels were modestly reduced in the *pyp1Δ* mutant (Fig 5C). The cAMP-PKA pathway-activated
290 transcriptional down-regulation of Nrg1 expression promotes yeast to hypha transition in *C.albicans* [38].
291 However, the *nrg1⁺* mRNA levels in a *S. japonicus* mutant lacking the single Pka1 catalytic subunit (*pka1Δ*)
292 [39] were similar to those present in wild type cells when growing in glucose-rich medium (Fig 5C),
293 suggesting that the cAMP-PKA pathway does not regulate Nrg1 expression in this organism. As compared to
294 untreated cells, *nrg1⁺* expression increased in wild type cells after 3h in the presence of CPT, and this rise was
295 much more evident in both *sty1Δ* and *atf1Δ* mutants (Fig 5D). Moreover, exogenous addition of QSMs
296 (phenylethanol 0.5 mM) partially reduced the enhanced expression of *nrg1⁺* in CPT-treated control and *sty1Δ*
297 cells, and quite strongly in *atf1Δ* cells (Fig 5D). Therefore, Nrg1 expression may be repressed via two
298 different/independent mechanisms, one involving Sty1-Atf1, and another mediated by QS.

299 The above findings draw a scenario where *S. japonicus* Nrg1 is an activator rather than a repressor of
300 hyphal growth. In support of this hypothesis, we found that both the average cell length and size distribution
301 of filamentous *nrg1Δ* cells after 6h of incubation with 0.2 μM CPT was lower than in wild type cells ($34 \pm$
302 $12,1 \mu\text{m}$ in *nrg1Δ* cells versus $43,8 \pm 18,4 \mu\text{m}$ in wild type cells) (Fig. 5E). Importantly, this phenotype was
303 accompanied by a significant reduction in the mycelial area expansion in *nrg1Δ* cells as compared to wild type
304 cells (Fig 5F). Indeed, simultaneous deletion of Nrg1 in *sty1Δ* cells (*nrg1Δ sty1Δ* double mutant) reduced, but

305 did not suppress, the increased mycelial expansion shown by the *sty1Δ* single mutant (Fig 5F). Hence, the
306 SAPK pathway may limit Nrg1 function as an activator of hyphal differentiation in *S. japonicus*.

307

308 **Discussion**

309 QS mediates developmental responses in several fungal species within the phylum Ascomycota,
310 including the subphyla Pezizomycotina (several *Aspergillus* species) and Saccharomycotina (budding yeasts
311 *S. cerevisiae* and *Debaryomyces hansenii*) [22, 23]. The demonstration of a QS brought about by aromatic
312 alcohols that inhibits *S. japonicus* hyphal development is, to our knowledge, the first description of such a
313 mechanism within the fission yeast clade (subphylum Taphrinomycotina). The yeast to hypha transition in
314 response to CPT is blocked in *S. japonicus* when the initial inoculum is $\geq 2 \cdot 10^6$ cells/ml, a value fairly similar
315 to that of *C. albicans*, which develops into filamentous forms during inducing conditions at densities $\leq 10^6$
316 cells/ml [22, 23]. Importantly, *S. japonicus* hyphal growth is strongly abolished in conditioned medium
317 obtained from high cell density cultures. An exhaustive compositional analysis of this medium identified
318 phenylethanol and tryptophol as the main QSMs of *S. japonicus*. Both compounds satisfy the main criteria
319 proposed to classify a molecule/s as true QSMs [22, 23]. They accumulate during the growth curve in a
320 density-dependent manner until reaching a maximum during the stationary phase. Moreover, their exogenous
321 addition limited yeast to hypha transition in liquid medium and reduced the mycelial expansion in solid
322 medium. Phenylethanol and tryptophol act as QSMs in *S. cerevisiae*, where they positively control
323 pseudohyphal and invasive filamentous morphology during nitrogen starvation [40]. Although similarly
324 produced in response to environmental changes, our findings suggest that the biological responses induced by
325 the above QSMs have evolved differently in these fungal species. Phenylethanol and tryptophol are also
326 produced by *C. albicans* in addition to farnesol, the major QSM that represses hyphal development in this
327 organism, but their putative role as QSMs is not clear [22, 23]. Repeated attempts failed to detect farnesol in
328 *S. japonicus* conditioned medium. However, we found out that addition of increased concentrations of this
329 aromatic alcohol that do not interfere with cell growth (5 to 40 μ M), significantly blocked *S. japonicus* hyphal
330 differentiation induced with CPT, and were able to reduce hyphal expansion in YEMA solid plates (Fig. S8).
331 Hence, farnesol behaves similarly as a QSM than the naturally produced phenylethanol and tryptophol to

332 block hyphal formation in this organism. The amount of chemically synthesized/purified phenylethanol and
333 tryptophol that elicit the QS mechanism (500-1000 μM) is higher than the maximal concentrations of both
334 compounds secreted by *S. japonicus* into rich medium (~ 10 to $100 \mu\text{M}$). This discrepancy, as reported in other
335 fungal species like *C. albicans* or *Cryptococcus neoformans* [41], might be related to either different
336 physicochemical and compositional nature of the conditioned medium (pH, nitrogen source,..), or to the
337 presence of other unknown metabolites that might synergize the QS effect of both aromatic alcohols. *S.*
338 *japonicus* releases important amounts of tyrosol into the growth medium ($\sim 75 \mu\text{M}$). However, similarly to *S.*
339 *cerevisiae* [40], this molecule does not appear to play a noticeable role during hyphal development.

340 The SAPK MAPK cascade governs multiple cellular events during vegetative growth and in response
341 to environmental changes *S. pombe*. Many of these functions, such as the cellular adaptation to stress
342 conditions and the sexual differentiation, are executed transcriptionally by Atf1, which becomes
343 phosphorylated and stabilized by activated Sty1 [42, 43]. Other roles are mostly prompted in a transcription-
344 independent manner and depend upon the ability of Sty1 to either activate or inhibit different substrates such
345 as cell cycle kinases, mRNA binding proteins, and translation factors [2, 30]. Like the equivalent *S. pombe*
346 mutants, *S. japonicus sty1* Δ and *atf1* Δ mutants are virtually sterile, and quickly lose viability when reaching
347 the stationary phase, indicating that the SAPK pathway positively regulates sexual differentiation and
348 chronological lifespan. Although showing a higher basal activity than in *S. pombe* during unperturbed growth,
349 Sty1 is strongly activated in *S. japonicus* in response to multiple stress situations, and *sty1* Δ and *atf1* Δ mutants
350 are growth sensitive under these conditions. Hence, even though *S. japonicus* displays some distinctive
351 biological features with regard to *S. pombe* [6-10], the core stress-responsive functions of the SAPK pathway
352 appear to be evolutionary conserved in both *Schizosaccharomyces* species. However, an unexpected exception
353 to this rule is the finding that, contrary to the *S. pombe* ortholog [44], Atf1 may positively regulate G2/M
354 progression in *S. japonicus*, since *atf1* Δ strain showed an increased cell size at division similar to that of the
355 *sty1* Δ mutant.

356 In contrast to *S. pombe*, *S. japonicus* undergoes robust hyphal development in response to
357 environmental cues [19]. Our results suggest that the SAPK pathway acts as a general negative regulator of
358 yeast to hypha transition in this organism. This conclusion is supported by several findings, such as the

359 increased presence of pseudohyphal cells and an invasive phenotype in *sty1Δ* and *atf1Δ* mutants, the increased
360 length of the hyphae and branching in these mutants during hyphal initiation as compared to wild type cells,
361 and the enhanced hyphal expansion displayed by the *sty1Δ* mutant in solid medium. Recently, it has been
362 show that *S. japonicus* mutants lacking the Sty1 activator MAPKK Wis1, but not Sty1 itself, shows increased
363 mycelial expansion [45]. This is a puzzling observation, since both kinases act in a linear pathway, and their
364 deletion should therefore give rise to highly similar, if not identical, cellular phenotypes. Moreover, we found
365 that cells lacking the tyrosine phosphatase Pyp1 that inactivates Sty1 were highly impaired in hyphal
366 development under both conditions, thus confirming the general role of the SAPK pathway in the negative
367 regulation of yeast to hypha transition.

368 In *S. japonicus* Sty1 and/or Atf1 appear to negatively regulate yeast to hyphal development both at the
369 transcriptional and post-translational levels. In *S. pombe* Atf1 becomes phosphorylated by Sty1 during stress
370 to induce the expression of CESR genes that modulate the adaptive cell response to the triggering stimuli [46].
371 However, a number of genes are also up- or down-regulated in *atf1Δ* cells under unperturbed conditions (low
372 Sty1 activity) [46], which suggests that Sty1 activation threshold prompts Atf1 to function either as a
373 repressor or as a transcriptional activator. This mechanism is likely conserved in *S. japonicus*, considering the
374 similar activation pattern of Sty1 in response to stress, and the conserved phenotypes of *sty1Δ* and *atf1Δ*
375 mutants. The fact that Sty1 activity is maintained at a basal level during the early stages of hyphal initiation,
376 together with the observation that both *sty1Δ* and *atf1Δ* cells are derepressed for filamentation in absence of
377 stimulus, indicate that the Sty1-Atf1 branch negatively controls the initial step of this developmental process
378 transcriptionally and in a constitutive fashion. However, Atf1 function seems less relevant during hyphal
379 growth and maintenance, since, contrary to the *sty1Δ* mutant, mycelial expansion is not enhanced in *atf1Δ*
380 cells. Sty1 might negatively regulate the later stages of hyphal growth transcriptionally and independently of
381 Atf1, at a post-translational level, or in both ways. The functional relationship between Sty1 and Atf1 during
382 control of this transition in *S. japonicus* somehow resembles that between the Sty1 ortholog Hog1 and the
383 transcriptional repressor Sko1 in *C. albicans*. In this organism the basal level of phosphorylated Hog1
384 represses the yeast to hypha development through Sko1 [47], which also serves as activator of genes induced
385 by stress [47, 48]. Indeed, both Hog1 and Sko1 repress yeast-to hypha transition and *hog1* and *sko1* mutants
386 display a hyperfilamentous phenotype under non-inducing conditions [49, 50]. In our model, the functional

387 relevance of the SAPK pathway as a constitutive repressor of dimorphism was further confirmed as Atf1 or
388 Sty1 deletion partially attenuated the QS mechanism that blocks hyphal development at high the cell densities.

389 The transcriptional repressor Nrg1 is a key negative regulator of hyphal initiation and maintenance in
390 *C. albicans*. whereas *nrg1* mutants constitutively grow as long pseudohyphae as the expression of hypha-
391 specific genes is constitutively derepressed [25, 26]. Hyphal initiation in *C. albicans* requires a quick and
392 temporary disappearance of Nrg1, whereas hyphal maintenance leads to exclusion of Nrg1 binding to
393 promoters of hypha-specific genes through a mechanism involving reduction in Hog1 activity [38].
394 Remarkably, in *S. japonicus* the Nrg1 ortholog is not a repressor but an activator of hyphal differentiation,
395 while the SAPK pathway may act as a major negative regulator of its expression and/or function. With respect
396 to control cells *nrg1*⁺ expression is up-regulated in both *sty1Δ* and *atf1Δ* mutants during vegetative growth and
397 hyphal initiation in response to CPT. Most important, Nrg1 absence elicited a reduction in cell filamentation
398 in response to CPT, and also in the mycelial area of expansion of both wild type and *sty1Δ* cells. Therefore,
399 repression of *nrg1*⁺ expression is biologically relevant during hyphal initiation and maintenance. However,
400 despite the large increase in *nrg1*⁺ expression in the *atf1Δ* mutant with respect to the wild type cells, mycelial
401 expansion is similar in both backgrounds, suggesting that Sty1 may also negatively regulate Nrg1 function
402 post-translationally. Nrg1 amino-acid sequence contains several putative–SP/TP and -PXSP/TP- MAPK
403 consensus phosphorylation sites (Fig. S7). It will be interesting to explore if whether Sty1 phosphorylates
404 Nrg1 *in vivo* and the biological impact on its function. From a broader perspective, another important issue
405 will be to elucidate the nature of the evolutionary structural and signaling constraints that define Nrg1 to
406 function either as activator (*S. japonicus*) or repressor (*C. albicans*) of hyphal growth in two distantly related
407 yeast species. Importantly, QS represses Nrg1 expression independently of the SAPK pathway, as shown by
408 the reducción in *nrg1*⁺ mRNA leves displayed by CPT-treated *sty1Δ* and *atf1Δ* cells in the presence of
409 phenylethanol (QSM).

410 In conclusion, our results show that QS and SAPK signaling are major negative regulators of the
411 dimorphic switch in *S. japonicus*. At low cellular densities the limited amount of QSMs in the growth medium
412 make QS not functional, and the SAPK pathway negatively controls hyphal differentiation by downregulating
413 elicitors of the yeast to hypha switch (Nrg1 and likely other factors) both transcriptionally and post-
414 transcriptionally. This control is bypassed in response to specific environmental cues as yeast cells commit

415 into hyphal growth. Contrariwise, increased presence of QSMs in high density cultures activates QS that
416 blocks hyphal differentiation in response to those stimuli. *S. japonicus* positions as an alternative and suitable
417 model organism to explore the intricate mechanisms regulating cellular differentiation in fungi.

418

419 **Materials and Methods**

420 ***Strains, growth conditions and reagents***

421 The *S. japonicus* strains used in this work derive from the original isolates described by Niki *et al.* [18], and
422 are listed in Table S9. For comparative studies the wild type *S. pombe* strain 972 (h⁻) was employed. They
423 were routinely grown with shaking at 30°C in rich (YES) or minimal (EMM2) medium with 2% glucose, and
424 supplemented with adenine, leucine, histidine, or uracil (100 mg/L, Sigma Chemical)[51]. In osmotic-saline
425 and oxidative stress experiments log-phase cultures (OD₆₀₀= 0.5; ~10⁶ cells/ml) were supplemented with either
426 KCl (Sigma-Aldrich) or hydrogen peroxide (Sigma-Aldrich), respectively. In glucose starvation experiments
427 cells grown in YES medium with 6% glucose were recovered by filtration, and resuspended in the same
428 medium lacking glucose and osmotically equilibrated with 3% glycerol. Log-phase cultures grown in YES
429 medium with 6% glucose were used in yeast to hyphae induction experiments with camptothecin (CPT,
430 Sigma-Aldrich) supplemented to a final concentration of 0.2 μM. YEMA [16] and RGE [27] media with 2%
431 agar were used to quantify mycelial growth. Chemically synthesized standards of phenylethanol, tyrosol, and
432 tryptophol were obtained from Sigma-Aldrich. Conditioned media were prepared by inoculating cells from
433 log-phase cultures (~10⁶ cels/ml) into fresh YES or YEMA medium to a final density of 5.10⁶, 5.10⁷, or 10⁸
434 cells/ml, incubated by 1-1.5h, and recovered by filtration.

435

436 ***Gene disruption***

437 Sequences of *S. japonicus* genes and those corresponding to *S. pombe* orthologs were obtained from the
438 annotated database at *EnsemblFungi*
439 (http://fungi.ensembl.org/Schizosaccharomyces_japonicus/Info/Index?db=core). The *S. japonicus* *sty1*⁺, *atf1*⁺,
440 *pyp1*⁺, *pka1*⁺ and *nrg1*⁺, null mutants were obtained by entire deletion of the corresponding coding sequences
441 by PCR-mediated strategy using plasmids pFK14 (*S. japonicus* *ura4*⁺ gene cloned into pGEMT-easy vector;

442 [52]) or pFA6a-*natMX6* [53] as templates , and their replacement with either *ura4*⁺ or *natMX6* cassettes
443 flanked by long 5' and 3' UTRs of respective genes following a PCR approach [54]. Oligonucleotides
444 employed to obtain each one of the transformation cassettes are shown in Table S10. *S. japonicus*
445 transformation by electroporation was performed exactly as described [55].

446

447 ***Quantification of mating efficiency***

448 Equivalent amounts (~10⁷ cells) of strains of the opposing mating type were mixed, poured on EMM2 plates
449 lacking nitrogen source (EMM2-N), and incubated at 28°C. The mating efficiency was determined after 24h
450 of incubation by microscopic counting of number of vegetative cells (V), zygotes (Z), and asci (A), according
451 to the following equation: % mating efficiency = (2Z+2A) x 100/(2Z+2A) + V. Triplicate samples (n_≥300
452 cells) were counted for each cross.

453

454 ***Plate assay of stress sensitivity for growth***

455 *S. japonicus* wild type and mutant strains were grown in YES liquid medium to OD₆₀₀= 0.5, and appropriate
456 decimal dilutions were spotted per duplicate on YES solid medium or in the same medium supplemented with
457 varying concentrations of potassium chloride, hydrogen peroxide, caffeine, and sodium dodecyl sulphate
458 (SDS; all purchased from Sigma). Plates were incubated at either 30 or 42°C for 3 days and then
459 photographed. All the assays were repeated at least three times with similar results. Representative
460 experiments are shown in the corresponding Figures.

461

462 ***Quantification of mycelial growth during nutritional stress***

463 Approximately 2.10⁶ cells from log-phase cultures (OD₆₀₀= 0.5) of wild type and mutant strains growing in
464 YES medium were spotted on YEMA or RGE plates, incubated at 30°C for 7 days, and then photographed and
465 saved as 16-bit .jpg digital images. The area of mycelial expansion was drawn by freehand for each strain
466 (n_≥6) and measured with the *analyze* tool using ImageJ [56].

467

468 ***cDNA synthesis and quantitative real time polymerase chain reaction (qPCR)***

469 *S. japonicus* wild type and mutant strains were grown in YES (6% glucose) in the absence or presence of CPT
470 (0.2 μ M) for the indicated times. Total RNAs were purified using the RNeasy mini kit (Qiagen), treated with
471 DNase (Invitrogen), and quantitated using Nanodrop 100 spectrophotometer (ThermoScientific). Total RNAs
472 (1 μ g) were reverse transcribed into cDNA with the iScript™ reverse transcription supermix (BioRad).
473 Quantitative real time polymerase chain reactions (qPCR) were performed using the iTaq™ Universal
474 SYBR® Green Supermix and a CFX96™ Real-Time PCR system (Bio-Rad Laboratories, CA, USA). Relative
475 gene expression was quantified based on $2^{-\Delta\Delta CT}$ method and normalized using *leu1*⁺ mRNA expression in each
476 sample. The list of gene-specific primers for qPCR is indicated in Table S9.

477

478 ***RNA sequencing and bioinformatics***

479 High quality DNA-free total RNAs (two biological replicates each; RIN value >8.0) were purified from wild
480 type, *sty1* Δ and *atf1* Δ mutants growing in YES medium to early log-phase (OD₆₀₀= 0.5). Total RNA was
481 extracted using the Ambion PureLink RNA Mini Kit according to manufacturers instructions Library
482 construction and sequencing was performed by BaseClear, Netherlands. The Illumina TruSeq RNA-seq
483 library preparation kit was used. Briefly, the mRNAs were purified by polyA capture, fragmented and
484 converted to double-stranded cDNA. DNA adapters were ligated to both ends of the DNA fragments and
485 subjected to PCR amplification. The sequence reads were generated using the Illumina HiSeq2500 system.
486 FASTQ read sequence files were generated using bcl2fastq2 (version 2.18). Initial quality assessment was
487 based on data passing the Illumina Chastity filtering. The second quality assessment was based on the
488 remaining reads using the FASTQC quality control tool (version 0.11.5). Tophat2 (version 2.1.1) [57] has
489 been used to align RNA-seq reads to the reference genome of *Schizosaccharomyces japonicus* (assembly:
490 GCA_000149845.2 at ENA/EMBL) . Cufflinks (version 2.2.1) [58] has been used to assemble the transcripts
491 and estimate their abundances. The data analysis and the graphical representations have been done using an
492 in-house R script . The NOISeq R package (version 2.24.0) [59] has been used for the differential expression
493 tests. The results were filtered using q-value=0,9 and FC=2. The enrichment analysis was performed using the
494 gProfileR R package (version 0.6.7) [60]. The *Schizosaccharomyces japonicus* GO annotation for biological
495 processes has been retrieved from Ensembl Fungi version 41 [61] using the biomaRt R package (version

496 2.36.1) [62]. Complete RNAseq data are available from the European Nucleotide Archive (ENA) database
497 (accession numbers ERS3040049, ERS3040050, ERS3040051, ERS3040052, ERS3040053, ERS3040054).

498

499 ***Detection and quantification of total and activated Sty1 levels***

500 In stress experiments cell extracts were prepared under native conditions employing chilled acid-washed glass
501 beads and lysis buffer (10% glycerol, 50 mM Tris HCl pH 7.5, 15 mM Imidazole, 150 mM NaCl, 0.1%
502 Nonidet NP-40, plus specific protease and phosphatase inhibitor, Sigma Chemical) [63]. In yeast to hypha
503 experiments with CPT cell extracts were obtained by trichloroacetic acid precipitation as described in [64].
504 Dual phosphorylation in Sty1 was detected employing mouse monoclonal anti-phospho-p38 antibody (Cell
505 Signaling). Total Sty1 levels were detected with rabbit polyclonal anti-Hog1 (y-215) antibody (Santa Cruz
506 Biotechnology Inc). Mouse monoclonal anti-PSTAIR (anti-Cdc2, Sigma-Aldrich) was used for loading
507 control. Immunoreactive bands were revealed with anti-rabbit or anti-mouse-HRP-conjugated secondary
508 antibodies (Sigma-Aldrich) and the ECL system (GE-Healthcare). Densitometric quantification of Western
509 blot signals as of 16-bit .jpg digital images of blots was performed using ImageJ [56]. Relative Units for Sty1
510 activation were estimated by determining the signal ratio of the anti-phospho-p38 blot (activated Sty1) with
511 respect to the anti-Hog1 blot (total Sty1) at each time point. Relative Units for total Sty1 were calculated by
512 determining the signal ratio of the anti-Hog1 blot (total Sty1) with respect to the anti-Cdc2 blot (loading
513 control). Unless otherwise stated, results shown correspond to experiments performed as biological triplicates.
514 Mean relative units \pm SD and/or representative results are shown. *P*-values were analyzed by unpaired
515 Student's *t* test.

516

517 ***Microscopy analysis***

518 Fluorescence images were obtained with a Leica DM4000B microscope equipped with a Leica DC400F
519 camera, and processed using IM500 Image Manager software. Calcofluor white and DAPI were employed,
520 respectively, for cell wall/septum and nuclei staining as described [51]. To determine cell length at division
521 the yeast strains were grown in YES medium to an A_{600} of 0.5 and stained with calcofluor white. A minimum
522 of 200 septated cells were scored per triplicate for each strain. To quantify the increase in cell length during
523 hyphal induction experiments with CPT, samples were taken at the indicated times and fixed immediately

524 with formaldehyde [65]. After staining with calcofluor white and/or DAPI the length of mononuclear late G2
525 cells ($n \geq 200$) was measured. Three biological replicates were scored for each strain genotype.

526

527 *GC/MS analysis.*

528 Phenylethanol in the conditioned medium was extracted with ethyl acetate at a ratio of 5:1, dried with N₂ at
529 room temperature, and resuspended in dichloromethane. The samples were analyzed by a GC 7890A (Agilent
530 Technologies, Santa Clara, CA, USA) coupled to a MS 5977 (Agilent Technologies, Santa Clara, CA, USA)
531 with an inert EI source and a Quadrupole detector. The column was a 30m Agilent Technologies HP
532 INNOWAX, 0.25 mm of internal diameter and 0.25 μ M of flow with an operating range from 40 to 270°C.
533 GC used a 1 μ l sample, injector and detector temperatures of 240 (splitless mode) and 150°C, respectively. The
534 oven temperature program started at 120°C, increased at 3°C/min to reach 220°C, and then at 10°C/min to
535 reach 250°C. The mass spectra were recorded in range of 35–300 m/z. Detection and quantification of
536 phenylethanol was performed in the extracted-ion chromatogram (EIC) selecting a characteristic ion
537 of m/z 91.

538

539 *HPLC/MS analysis.*

540 The detection and quantification of tyrosol and tryptophol in conditioned medium was determined with a
541 HPLC/MS system consisting of a 1290 Infinity II Series HPLC (Agilent Technologies, Santa Clara, CA,
542 USA), and connected to a 6550 Q-TOF Mass Spectrometer (Agilent Technologies, Santa Clara, CA, USA)
543 using an Agilent Jet Stream Dual electrospray (AJS-Dual ESI) interface. Aromatic alcohols in 1 ml samples
544 from conditioned medium were extracted with 3 ml of ethyl-acetate and vortexed for 1 min. After centrifuging
545 for 5 min, the organic phase was transferred to a new tube, evaporated, and resuspended in 100 μ l of MilliQ
546 water. Aromatic alcohol standards were dissolved in ethanol. Samples and standards (20 μ l each) were injected
547 into a Waters XBridge C18 HPLC column (2.1 \times 100 mm, 5 μ m, Agilent Technologies), thermostated at
548 30°C, and eluted at a flow rate of 400 μ l/min. Mobile phase A (0.1% formic acid (w/v) in MilliQ water), and
549 mobile phase B (0.1% formic acid (w/v) in acetonitrile), were used for the chromatographic separation. The
550 initial HPLC running conditions were solvent A:B 95:5 (v/v). The gradient elution program was 5% solvent B

551 for 3 min; a linear gradient from 5 to 100% solvent B in 10 min; 2 min at constant 100% solvent B. The mass
552 spectrometer was operated in the positive mode. Profile data were acquired for both MS and MS/MS scans in
553 extended dynamic range mode. MS and MS/MS mass range was 50-250 m/z and scan rates were 8 spectra/sec
554 for MS and 3 spectra/sec for MS/MS. Tyrosol was detected as the 130.1591 m/z, whereas tryptophol was
555 detected as the [M+H]⁺ ion at 162.0909 m/z, and confirmed with the transition 162.0909 > 144.0807.

556

557 ***HPLC/UV analysis.***

558 Alternatively, concentrations of 2-phenyl ethanol, tyrosol and tryptophol in conditioned medium were
559 determined using an Agilent 1100 Series high-performance liquid chromatography system (HPLC, Agilent
560 Technologies, Santa Clara, CA, USA) equipped with a thermostated μ -wellplate autosampler, a quaternary
561 pump, and a multiple wavenumber detector. Samples and standards (40 μ l) were injected into a Zorbax
562 Eclipse XDB-C18 HPLC column (Agilent Technologies), thermostated at 30°C, and eluted at a flow rate of
563 400 μ l/min. Mobile phase A (0.1% acetic acid (w/v) in MilliQ water) and mobile phase B (0.1% formic acid
564 (w/v) in methanol), were used for the chromatographic separation. The initial HPLC running conditions were
565 solvent A:B 95:5 (v/v). The gradient elution program was 5% solvent B for 5 min; a linear gradient from 5 to
566 100% solvent B in 20 min; 5 min at constant 100% solvent B. The detection wavelength was 210 nm.

567

568 **Acknowledgements**

569 Members of the yeast physiology group wish to dedicate this work to Professor Mariano Gacto on the
570 occasion of his retirement. We thank Professor Hironori Niki for *S. japonicus* yeast strains and plasmids, and
571 to F. Garro for technical assistance. Thanks to José Rodríguez and Alejandro Torrecillas for their invaluable
572 help with gas chromatography/mass spec and liquid chromatography/mass spec analysis, respectively. Thanks
573 to Pilar Pérez and Jaime Correa-Bordes for many helpful discussions and comments on the manuscript, and to
574 Esther Guarinos for language revision. Elisa Gómez-Gil is a PhD fellow (FPI program) from the University of
575 Murcia, Spain. This work was supported by grants from Ministerio de Economía y Competitividad
576 (BFU2017-82423-P), and Fundación Séneca-Region de Murcia (20856/PI/18), Spain. European Regional
577 Development Fund (ERDF) co-funding from the European Union.

579 **References**

- 580 1. Bluthgen N, Legewie S. Systems analysis of MAPK signal transduction. *Essays Biochem.* 2008;45:95-107.
581 Epub 2008/09/17. doi: 10.1042/bse0450095. PubMed PMID: 18793126.
- 582 2. Perez P, Cansado J. Cell Integrity Signaling and Response to Stress in Fission Yeast. *Current Protein & Peptide*
583 *Science.* 2010;11(8):680-92. doi: 10.2174/138920310794557718. PubMed PMID: WOS:000287357000005.
- 584 3. Mutavchiev DR, Leda M, Sawin KE. Remodeling of the Fission Yeast Cdc42 Cell-Polarity Module via the Sty1
585 p38 Stress-Activated Protein Kinase Pathway. *Curr Biol.* 2016;26(21):2921-8. Epub 2016/10/18. doi:
586 10.1016/j.cub.2016.08.048. PubMed PMID: 27746023; PubMed Central PMCID: PMC5106388.
- 587 4. Klar AJ. *Schizosaccharomyces japonicus* yeast poised to become a favorite experimental organism for
588 eukaryotic research. *G3 (Bethesda).* 2013;3(10):1869-73. Epub 2013/08/13. doi: 10.1534/g3.113.007187. PubMed
589 PMID: 23934997; PubMed Central PMCID: PMC3789812.
- 590 5. Rhind N, Chen Z, Yassour M, Thompson DA, Haas BJ, Habib N, et al. Comparative functional genomics of the
591 fission yeasts. *Science.* 2011;332(6032):930-6. Epub 2011/04/23. doi: 10.1126/science.1203357. PubMed PMID:
592 21511999; PubMed Central PMCID: PMC3131103.
- 593 6. Yam C, He Y, Zhang D, Chiam KH, Oliferenko S. Divergent strategies for controlling the nuclear membrane
594 satisfy geometric constraints during nuclear division. *Curr Biol.* 2011;21(15):1314-9. Epub 2011/08/02. doi:
595 10.1016/j.cub.2011.06.052. PubMed PMID: 21802294.
- 596 7. Gu Y, Yam C, Oliferenko S. Divergence of mitotic strategies in fission yeasts. *Nucleus.* 2012;3(3):220-5. Epub
597 2012/05/11. doi: 10.4161/nucl.19514. PubMed PMID: 22572960; PubMed Central PMCID: PMC3414397.
- 598 8. Gu Y, Oliferenko S. Comparative biology of cell division in the fission yeast clade. *Curr Opin Microbiol.*
599 2015;28:18-25. Epub 2015/08/12. doi: 10.1016/j.mib.2015.07.011. PubMed PMID: 26263485.
- 600 9. Kaino T, Tonoko K, Mochizuki S, Takashima Y, Kawamukai M. *Schizosaccharomyces japonicus* has low levels
601 of CoQ10 synthesis, respiration deficiency, and efficient ethanol production. *Biosci Biotechnol Biochem.*
602 2018;82(6):1031-42. Epub 2017/12/02. doi: 10.1080/09168451.2017.1401914. PubMed PMID: 29191091.
- 603 10. Chew TG, Huang J, Palani S, Sommese R, Kamnev A, Hatano T, et al. Actin turnover maintains actin filament
604 homeostasis during cytokinetic ring contraction. *J Cell Biol.* 2017;216(9):2657-67. Epub 2017/06/29. doi:
605 10.1083/jcb.201701104. PubMed PMID: 28655757; PubMed Central PMCID: PMC5584170.
- 606 11. Alfa CE, Hyams JS. Distribution of tubulin and actin through the cell division cycle of the fission yeast
607 *Schizosaccharomyces japonicus* var. *versatilis*: a comparison with *Schizosaccharomyces pombe*. *J Cell Sci.* 1990;96 (Pt
608 1):71-7. PubMed PMID: 2197287.
- 609 12. Aoki K, Hayashi H, Furuya K, Sato M, Takagi T, Osumi M, et al. Breakage of the nuclear envelope by an
610 extending mitotic nucleus occurs during anaphase in *Schizosaccharomyces japonicus*. *Genes Cells.* 2011;16(9):911-26.
611 Epub 2011/07/08. doi: 10.1111/j.1365-2443.2011.01540.x. PubMed PMID: 21733045.
- 612 13. Amoah-Buahin E, Bone N, Armstrong J. Hyphal Growth in the Fission Yeast *Schizosaccharomyces pombe*.
613 *Eukaryot Cell.* 2005;4(7):1287-97. Epub 2005/07/09. doi: 10.1128/ec.4.7.1287-1297.2005. PubMed PMID: 16002654;
614 PubMed Central PMCID: PMC1168962.
- 615 14. Dodgson J, Avula H, Hoe KL, Kim DU, Park HO, Hayles J, et al. Functional genomics of adhesion, invasion,
616 and mycelial formation in *Schizosaccharomyces pombe*. *Eukaryot Cell.* 2009;8(8):1298-306. Epub 2009/06/23. doi:
617 10.1128/ec.00078-09. PubMed PMID: 19542312; PubMed Central PMCID: PMC2725560.
- 618 15. Dodgson J, Brown W, Rosa CA, Armstrong J. Reorganization of the growth pattern of *Schizosaccharomyces*
619 *pombe* in invasive filament formation. *Eukaryot Cell.* 2010;9(11):1788-97. Epub 2010/09/28. doi: 10.1128/ec.00084-10.
620 PubMed PMID: 20870879; PubMed Central PMCID: PMC2976291.
- 621 16. Sipiczki M, Takeo K, Yamaguchi M, Yoshida S, Miklos I. Environmentally controlled dimorphic cycle in a
622 fission yeast. *Microbiology.* 1998;144 (Pt 5):1319-30. Epub 1998/06/05. doi: 10.1099/00221287-144-5-1319. PubMed
623 PMID: 9611807.
- 624 17. Papp L, Sipiczki M, Holb IJ, Miklos I. Optimal conditions for mycelial growth of *Schizosaccharomyces*
625 *japonicus* cells in liquid medium: it enables the molecular investigation of dimorphism. *Yeast.* 2014;31(12):475-82. Epub
626 2014/10/14. doi: 10.1002/yea.3048. PubMed PMID: 25308606.
- 627 18. Aoki K, Furuya K, Niki H. *Schizosaccharomyces japonicus*: A Distinct Dimorphic Yeast among the Fission
628 Yeasts. *Cold Spring Harb Protoc.* 2017;2017(12):pdb.top082651. Epub 2017/07/25. doi: 10.1101/pdb.top082651.
629 PubMed PMID: 28733412.
- 630 19. Niki H. Induction of Hyphal Growth in *Schizosaccharomyces japonicus*. *Cold Spring Harb Protoc.*
631 2017;2017(12):pdb.prot091868. Epub 2017/07/25. doi: 10.1101/pdb.prot091868. PubMed PMID: 28733395.
- 632 20. Furuya K, Niki H. The DNA damage checkpoint regulates a transition between yeast and hyphal growth in
633 *Schizosaccharomyces japonicus*. *Mol Cell Biol.* 2010;30(12):2909-17. Epub 2010/04/07. doi: 10.1128/mcb.00049-10.
634 PubMed PMID: 20368354; PubMed Central PMCID: PMC2876669.

- 635 21. Furuya K, Niki H. Hyphal differentiation induced via a DNA damage checkpoint-dependent pathway engaged in
636 crosstalk with nutrient stress signaling in *Schizosaccharomyces japonicus*. *Curr Genet*. 2012;58(5-6):291-303. Epub
637 2012/10/24. doi: 10.1007/s00294-012-0384-4. PubMed PMID: 23090706; PubMed Central PMCID: PMCPCMC3490063.
- 638 22. Albuquerque P, Casadevall A. Quorum sensing in fungi--a review. *Med Mycol*. 2012;50(4):337-45. Epub
639 2012/01/25. doi: 10.3109/13693786.2011.652201. PubMed PMID: 22268493; PubMed Central PMCID:
640 PMCPCMC4294699.
- 641 23. Wongsuk T, Pumeesat P, Luplertlop N. Fungal quorum sensing molecules: Role in fungal morphogenesis and
642 pathogenicity. *J Basic Microbiol*. 2016;56(5):440-7. Epub 2016/03/15. doi: 10.1002/jobm.201500759. PubMed PMID:
643 26972663.
- 644 24. González Villa T, Vinas M, SpringerLink (Online service). *New Weapons to Control Bacterial Growth*. 1st ed.
645 Cham: Imprint Springer; 2016. 1 recurso en línea p.
- 646 25. Braun BR, Kadosh D, Johnson AD. NRG1, a repressor of filamentous growth in *C.albicans*, is down-regulated
647 during filament induction. *Embo j*. 2001;20(17):4753-61. Epub 2001/09/05. doi: 10.1093/emboj/20.17.4753. PubMed
648 PMID: 11532939; PubMed Central PMCID: PMCPCMC125265.
- 649 26. Murad AM, Leng P, Straffon M, Wishart J, Macaskill S, MacCallum D, et al. NRG1 represses yeast-hypha
650 morphogenesis and hypha-specific gene expression in *Candida albicans*. *Embo j*. 2001;20(17):4742-52. Epub
651 2001/09/05. doi: 10.1093/emboj/20.17.4742. PubMed PMID: 11532938; PubMed Central PMCID: PMCPCMC125592.
- 652 27. Kinnaer C, Dudin O, Martin SG. Yeast-to-hypha transition of *Schizosaccharomyces japonicus* in response to
653 environmental stimuli. *Mol Biol Cell*. 2019;30(8):975-91. Epub 2019/02/06. doi: 10.1091/mbc.E18-12-0774. PubMed
654 PMID: 30726171.
- 655 28. Nguyen T, Ruan Z, Oruganty K, Kannan N. Co-conserved MAPK features couple D-domain docking groove to
656 distal allosteric sites via the C-terminal flanking tail. *PLoS One*. 2015;10(3):e0119636. Epub 2015/03/24. doi:
657 10.1371/journal.pone.0119636. PubMed PMID: 25799139; PubMed Central PMCID: PMCPCMC4370755.
- 658 29. Clotet J, Posas F. Control of cell cycle in response to osmotic stress: lessons from yeast. *Methods Enzymol*.
659 2007;428:63-76. Epub 2007/09/19. doi: 10.1016/s0076-6879(07)28004-8. PubMed PMID: 17875412.
- 660 30. Lopez-Aviles S, Grande M, Gonzalez M, Helgesen AL, Alemany V, Sanchez-Piris M, et al. Inactivation of the
661 Cdc25 phosphatase by the stress-activated *Srk1* kinase in fission yeast. *Mol Cell*. 17. United States2005. p. 49-59.
- 662 31. Petersen J, Hagan IM. Polo kinase links the stress pathway to cell cycle control and tip growth in fission yeast.
663 *Nature*. 435. England2005. p. 507-12.
- 664 32. Zuin A, Carmona M, Morales-Ivorra I, Gabrielli N, Vivancos AP, Ayte J, et al. Lifespan extension by calorie
665 restriction relies on the *Sty1* MAP kinase stress pathway. *EMBO J*. 29. England2010. p. 981-91.
- 666 33. Madrid M, Soto T, Franco A, Paredes V, Vicente J, Hidalgo E, et al. A cooperative role for *Atf1* and *Pap1* in the
667 detoxification of the oxidative stress induced by glucose deprivation in *Schizosaccharomyces pombe*. *Journal of*
668 *Biological Chemistry*. 2004;279(40):41594-602. doi: 10.1074/jbc.M405509200. PubMed PMID:
669 WOS:000224075500044.
- 670 34. Quinn J, Findlay VJ, Dawson K, Millar JB, Jones N, Morgan BA, et al. Distinct regulatory proteins control the
671 graded transcriptional response to increasing H_2O_2 levels in fission yeast *Schizosaccharomyces pombe*. *Mol Biol*
672 *Cell*. 2002;13(3):805-16. Epub 2002/03/22. doi: 10.1091/mbc.01-06-0288. PubMed PMID: 11907263; PubMed Central
673 PMCID: PMCPCMC99600.
- 674 35. Wilkinson MG, Samuels M, Takeda T, Toone WM, Shieh JC, Toda T, et al. The *Atf1* transcription factor is a
675 target for the *Sty1* stress-activated MAP kinase pathway in fission yeast. *Genes Dev*. 1996;10(18):2289-301. Epub
676 1996/09/15. PubMed PMID: 8824588.
- 677 36. Gao J, Davidson MK, Wahls WP. Distinct regions of ATF/CREB proteins *Atf1* and *Pcr1* control recombination
678 hotspot *ade6-M26* and the osmotic stress response. *Nucleic Acids Res*. 36. England2008. p. 2838-51.
- 679 37. Kuchin S, Vyas VK, Carlson M. *Snf1* protein kinase and the repressors *Nrg1* and *Nrg2* regulate *FLO11*, haploid
680 invasive growth, and diploid pseudohyphal differentiation. *Mol Cell Biol*. 2002;22(12):3994-4000. Epub 2002/05/25.
681 PubMed PMID: 12024013; PubMed Central PMCID: PMCPCMC133850.
- 682 38. Lu Y, Su C, Liu H. *Candida albicans* hyphal initiation and elongation. *Trends Microbiol*. 2014;22(12):707-14.
683 Epub 2014/09/30. doi: 10.1016/j.tim.2014.09.001. PubMed PMID: 25262420; PubMed Central PMCID:
684 PMCPCMC4256103.
- 685 39. Papp L, Sipiczki M, Miklos I. Expression pattern and phenotypic characterization of the mutant strain reveals
686 target genes and processes regulated by *pka1* in the dimorphic fission yeast *Schizosaccharomyces japonicus*. *Curr Genet*.
687 2017;63(3):487-97. Epub 2016/09/30. doi: 10.1007/s00294-016-0651-x. PubMed PMID: 27678009.
- 688 40. Chen H, Fink GR. Feedback control of morphogenesis in fungi by aromatic alcohols. *Genes Dev*.
689 2006;20(9):1150-61. Epub 2006/04/19. doi: 10.1101/gad.1411806. PubMed PMID: 16618799; PubMed Central PMCID:
690 PMCPCMC1472474.
- 691 41. Albuquerque P, Nicola AM, Nieves E, Paes HC, Williamson PR, Silva-Pereira I, et al. Quorum sensing-
692 mediated, cell density-dependent regulation of growth and virulence in *Cryptococcus neoformans*. *MBio*.
693 2013;5(1):e00986-13. Epub 2014/01/02. doi: 10.1128/mBio.00986-13. PubMed PMID: 24381301; PubMed Central
694 PMCID: PMCPCMC3884061.

- 695 42. Sanso M, Gogol M, Ayte J, Seidel C, Hidalgo E. Transcription factors Pcr1 and Atf1 have distinct roles in
696 stress- and Sty1-dependent gene regulation. *Eukaryot Cell*. 7. United States2008. p. 826-35.
- 697 43. Lawrence CL, Maekawa H, Worthington JL, Reiter W, Wilkinson CR, Jones N. Regulation of
698 *Schizosaccharomyces pombe* Atf1 protein levels by Sty1-mediated phosphorylation and heterodimerization with Pcr1. *J*
699 *Biol Chem*. 282. United States2007. p. 5160-70.
- 700 44. Shiozaki K, Russell P. Conjugation, meiosis, and the osmotic stress response are regulated by Spc1 kinase
701 through Atf1 transcription factor in fission yeast. *Genes Dev*. 1996;10(18):2276-88. Epub 1996/09/15. PubMed PMID:
702 8824587.
- 703 45. Nozaki S, Furuya K, Niki H. The Ras1-Cdc42 pathway is involved in hyphal development of
704 *Schizosaccharomyces japonicus*. *FEMS Yeast Res*. 2018;18(4). Epub 2018/03/23. doi: 10.1093/femsyr/foy031. PubMed
705 PMID: 29566183.
- 706 46. Chen D, Toone WM, Mata J, Lyne R, Burns G, Kivinen K, et al. Global transcriptional responses of fission
707 yeast to environmental stress. *Mol Biol Cell*. 2003;14(1):214-29. Epub 2003/01/17. doi: 10.1091/mbc.e02-08-0499.
708 PubMed PMID: 12529438; PubMed Central PMCID: PMCPMC140239.
- 709 47. Alonso-Monge R, Román E, Arana DM, Prieto D, Urrialde V, Nombela C, et al. The Sko1 protein represses the
710 yeast-to-hypha transition and regulates the oxidative stress response in *Candida albicans*. *Fungal Genet Biol*.
711 2010;47(7):587-601. Epub 2010/04/11. doi: 10.1016/j.fgb.2010.03.009. PubMed PMID: 20388546.
- 712 48. Rauceo JM, Blankenship JR, Fanning S, Hamaker JJ, Deneault JS, Smith FJ, et al. Regulation of the *Candida*
713 *albicans* cell wall damage response by transcription factor Sko1 and PAS kinase Psk1. *Mol Biol Cell*. 2008;19(7):2741-
714 51. Epub 2008/04/23. doi: 10.1091/mbc.e08-02-0191. PubMed PMID: 18434592; PubMed Central PMCID:
715 PMCPMC2441657.
- 716 49. Alonso-Monge R, Navarro-García F, Molero G, Diez-Orejas R, Gustin M, Pla J, et al. Role of the mitogen-
717 activated protein kinase Hog1p in morphogenesis and virulence of *Candida albicans*. *J Bacteriol*. 1999;181(10):3058-68.
718 PubMed PMID: 10322006; PubMed Central PMCID: PMCPMC93760.
- 719 50. Eisman B, Alonso-Monge R, Román E, Arana D, Nombela C, Pla J. The Cek1 and Hog1 mitogen-activated
720 protein kinases play complementary roles in cell wall biogenesis and chlamydospore formation in the fungal pathogen
721 *Candida albicans*. *Eukaryot Cell*. 2006;5(2):347-58. doi: 10.1128/EC.5.2.347-358.2006. PubMed PMID: 16467475;
722 PubMed Central PMCID: PMCPMC1405885.
- 723 51. Moreno S, Klar A, Nurse P. Molecular Genetic-Analysis Of Fission Yeast *Schizosaccharomyces pombe*.
724 *Methods in Enzymology*. 1991;194:795-823. PubMed PMID: WOS:A1991FN84200056.
- 725 52. Furuya K, Niki H. Isolation of heterothallic haploid and auxotrophic mutants of *Schizosaccharomyces*
726 *japonicus*. *Yeast*. 2009;26(4):221-33. Epub 2009/03/31. doi: 10.1002/yea.1662. PubMed PMID: 19330769.
- 727 53. Hentges P, Van Driessche B, Tafforeau L, Vandenhoute J, Carr AM. Three novel antibiotic marker cassettes for
728 gene disruption and marker switching in *Schizosaccharomyces pombe*. *Yeast*. 2005;22(13):1013-9. doi:
729 10.1002/yea.1291. PubMed PMID: 16200533.
- 730 54. Krawchuk MD, Wahls WP. High-efficiency gene targeting in *Schizosaccharomyces pombe* using a modular,
731 PCR-based approach with long tracts of flanking homology. *Yeast*. 1999;15(13):1419-27. doi: 10.1002/(SICI)1097-
732 0061(19990930)15:13<1419::AID-YEA466>3.0.CO;2-Q. PubMed PMID: 10509024; PubMed Central PMCID:
733 PMCPMC3190138.
- 734 55. Aoki K, Niki H. Transformation of *Schizosaccharomyces japonicus*. *Cold Spring Harb Protoc*.
735 2017;2017(12):pdb.prot091850. Epub 2017/07/25. doi: 10.1101/pdb.prot091850. PubMed PMID: 28733403.
- 736 56. Schneider C, Rasband W, Eliceiri K. NIH Image to ImageJ: 25 years of image analysis. *Nature Methods*.
737 2012;9(7):671-5. doi: 10.1038/nmeth.2089. PubMed PMID: WOS:000305942200020.
- 738 57. Kim D, Pertea G, Trapnell C, Pimentel H, Kelley R, Salzberg SL. TopHat2: accurate alignment of
739 transcriptomes in the presence of insertions, deletions and gene fusions. *Genome Biology*. 2013;14(4). doi: 10.1186/gb-
740 2013-14-4-r36. PubMed PMID: WOS:000322521300006.
- 741 58. Trapnell C, Roberts A, Goff L, Pertea G, Kim D, Kelley DR, et al. Differential gene and transcript expression
742 analysis of RNA-seq experiments with TopHat and Cufflinks (vol 7, pg 562, 2012). *Nature Protocols*. 2014;9(10):2513-
743 doi: 10.1038/nprot1014-2513a. PubMed PMID: WOS:000343227800017.
- 744 59. Tarazona S, Furio-Tari P, Turra D, Di Pietro A, Jose Nueda M, Ferrer A, et al. Data quality aware analysis of
745 differential expression in RNA-seq with NOISeq R/Bioc package. *Nucleic Acids Research*. 2015;43(21). doi:
746 10.1093/nar/gkv711. PubMed PMID: WOS:000366410900003.
- 747 60. Reimand J, Arak T, Adler P, Kolberg L, Reisberg S, Peterson H, et al. g:Profiler-a web server for functional
748 interpretation of gene lists (2016 update). *Nucleic Acids Research*. 2016;44(W1):W83-W9. doi: 10.1093/nar/gkw199.
749 PubMed PMID: WOS:000379786800015.
- 750 61. Kersey PJ, Allen JE, Allot A, Barba M, Boddu S, Bolt BJ, et al. Ensembl Genomes 2018: an integrated omics
751 infrastructure for non-vertebrate species. *Nucleic Acids Research*. 2018;46(D1):D802-D8. doi: 10.1093/nar/gkx1011.
752 PubMed PMID: WOS:000419550700119.

- 753 62. Durinck S, Spellman PT, Birney E, Huber W. Mapping identifiers for the integration of genomic datasets with
754 the R/Bioconductor package biomaRt. *Nature Protocols*. 2009;4(8):1184-91. doi: 10.1038/nprot.2009.97. PubMed
755 PMID: WOS:000268858800008.
- 756 63. Madrid M, Jimenez R, Sanchez-Mir L, Soto T, Franco A, Vicente-Soler J, et al. Multiple layers of regulation
757 influence cell integrity control by the PKC ortholog Pck2 in fission yeast. *J Cell Sci*. 128. England: 2015. Published by
758 The Company of Biologists Ltd.; 2015. p. 266-80.
- 759 64. Grallert A, Hagan IM. Preparation of Protein Extracts from *Schizosaccharomyces pombe* Using Trichloroacetic
760 Acid Precipitation. *Cold Spring Harb Protoc*. 2017;2017(2). Epub 2017/02/01. doi: 10.1101/pdb.prot091579. PubMed
761 PMID: 28148851.
- 762 65. Hagan IM. Immunofluorescence Microscopy of *Schizosaccharomyces pombe* Using Chemical Fixation. *Cold*
763 *Spring Harb Protoc*. 2016;2016(7). Epub 2016/07/01. doi: 10.1101/pdb.prot091017. PubMed PMID: 27371599.
764
765

766 **Figure legends**

767 **Fig. 1.** Quorum sensing negatively regulates yeast to hypha transition in *S. japonicus*.

768 (A) Exponentially growing *S. japonicus* wild type cells were recovered by filtration, inoculated at the
769 indicated initial cell densities in high glucose (6%) YES medium, and incubated for 6h in the presence or
770 absence of 0.2 μ M CPT. Cell length is represented as box and whisker plots. Data obtained after quantification
771 of one experiment performed per triplicate ($n \geq 200$ cells/strain) is shown. *****, $P < 0.0001$, as calculated by
772 unpaired Student's *t* test. Fixed cells from representative experiments were stained with calcofluor white and
773 observed by fluorescence microscopy. Scale bar: 10 μ m. (B) *S. japonicus* wild type cells were inoculated at
774 low density (10^6 cells/ml) in fresh YES medium (3% glucose) or in filter-sterilized conditioned medium (~3%
775 remaining glucose concentration) obtained from a culture of the same strain growing to high cell density
776 ($\geq 10^8$ cells/ml), and supplemented with 0.2 μ M CPT. Aliquots were recovered after 6h of incubation, stained
777 with calcofluor white, and the percentage of elongated/hyphal cells was determined by fluorescence
778 microscopy. Data are expressed as mean \pm SD and correspond to biological triplicates ($n \geq 200$ cells/sample).
779 **, $P < 0.005$, as calculated by unpaired Student's *t* test. (C) Cell length represented as box and whisker plots in
780 *S. japonicus* wild type cells growing exponentially for 6h in the presence of 0.2 μ M CPT in either fresh
781 (unconditioned) or conditioned YES medium (3% glucose) obtained from a culture of the same strain growing
782 at a density of $5 \cdot 10^6$, $5 \cdot 10^7$ or 10^8 cells/ml. The experiment was performed per triplicate ($n \geq 200$ cells) and
783 quantification of one is shown. *****, $P < 0.0001$, as calculated by unpaired Student's *t* test. CPT-treated cells
784 growing in unconditioned and conditioned medium (density of $5 \cdot 10^7$ cells/ml) stained with calcofluor white
785 and observed by fluorescence microscopy. Scale bar: 10 μ m. (D) Cells from *S. japonicus* wild type cells
786 growing in YES medium ($2 \cdot 10^6$) were spotted on YEMA plates prepared with unconditioned or conditioned
787 medium obtained from a culture of the same strain growing to a density of $5 \cdot 10^6$ or $5 \cdot 10^7$ cells/ml, incubated at
788 30°C for 7 days, and then photographed. The total area of mycelial expansion (expressed as relative units) was
789 measured ($n > 6$) and is represented as scatter plot. *****, $P < 0.0001$, as calculated by unpaired Student's *t* test.
790 (E) Growth curve of wild type *S. japonicus* in high glucose (6%) YES medium was followed by determining
791 OD_{600} values at different times (black circles). Media supernatants were recovered by filter-sterilization at the
792 indicated time points, and the concentration of phenylethanol (black bars), tyrosol (grey bars), and tryptophol

793 (white bars) secreted into the growth medium was determined by GC/MS or HPLC/MS analysis. Data are
794 expressed as mean \pm SD and correspond to biological triplicates.
795 (F) Exponentially growing *S. japonicus* wild type cells were inoculated at an initial cell density of 10^6 cells/ml
796 in high glucose (6%) YES medium and incubated for 6h with 0.2 μ M CPT without further treatment
797 (untreated) or in the presence of the indicated amounts of either phenylethanol, tyrosol, tryptophol, or
798 phenylethanol plus tryptophol. Cell length is represented as box and whisker plots. Data obtained after
799 quantification of one experiment performed per triplicate ($n \geq 200$ cells/sample) is shown. ****, $P < 0.0001$; ns,
800 not significant, as calculated by unpaired Student's *t* test. (G) Cells from *S. japonicus* wild type cells growing
801 in YES medium ($2 \cdot 10^6$) were spotted on YEMA or RGE plates in the absence or presence of the indicated
802 amounts of either phenylethanol, tyrosol, tryptophol, or phenylethanol plus tryptophol, incubated at 30°C for 7
803 days, and then photographed. The total area of mycelial expansion (expressed as relative units) was measured
804 ($n \geq 6$) and is represented as scatter plot. *, $P < 0.05$; ***, $P < 0.001$; ns, not significant, as calculated by unpaired
805 Student's *t* test.

806

807 **Fig. 2.** The stress-regulatory functions of the SAPK pathway are conserved in *S. japonicus*.

808 (A) Cell length at division represented as box and whisker plots in *S. japonicus* wild type, *sty1* Δ , *pyp1* Δ and
809 *atf1* Δ mutants. Experiment was performed per triplicate ($n \geq 200$ cells/strain) and quantification of one is
810 shown. ****, $P < 0.0001$, as calculated by unpaired Student's *t* test. Cell morphology of each strain was
811 analyzed by fluorescence microscopy after staining with calcofluor white. Scale bar: 10 μ m. (B) *S. japonicus*
812 wild type, *sty1* Δ and *atf1* Δ mutants of the h^+ mating type were mixed with wild type h^- cells, poured on
813 EMM2-N plates, and incubated at 28°C. The percentage of conjugation efficiency (as mean \pm SD) was
814 determined after 24h of incubation by microscopic counting of number of vegetative cells, zygotes, and asci.
815 Biological triplicate samples ($n \geq 300$ cells) were counted for each cross. ***, $P < 0.005$; ****, $P < 0.001$, as
816 calculated by unpaired Student's *t* test. (C) Wild type *S. pombe* and *S. japonicus* strains were grown in YES
817 medium to mid-log phase. Activated/total Sty1 were detected with anti-phospho-p38 and anti-Hog1 antibodies,
818 respectively. Anti-cdc2 was used as loading control. Relative units as mean \pm SD (biological triplicates) for
819 Sty1 phosphorylation (anti-phospho-p38 blot) were determined with respect to the internal control (anti-Hog1
820 blot). *, $P < 0.05$, as calculated by unpaired Student's *t* test. (D) Wild type *S. pombe* and *S. japonicus* strains

821 were grown in YES medium to mid-log phase, and treated with either 0.6 M KCl (upper left panel), 1 mM
822 H₂O₂ (lower left panel), incubated at 40°C (*S. pombe*) or 45°C (*S. japonicus*) (upper right panel), and shifted to
823 the same medium without glucose and supplemented with 3% glycerol (lower right panel). Activated/total
824 Sty1 were detected with anti-phospho-p38 and anti-Hog1 antibodies, respectively. Anti-cdc2 was used as
825 loading control. Relative units as mean \pm SD (biological triplicates) for Sty1 phosphorylation (anti-phospho-
826 p38 blot) were determined with respect to the internal control (anti-Hog1 blot). (E) Serially diluted cells of
827 wild type, *sty1* Δ and *atf1* Δ strains were spotted on YES plates supplemented with either 1.2 M KCl, 1.5 mM
828 H₂O₂, 6 mM caffeine, or 0.01% SDS, and incubated for 3 days at either 30 or 42°C. Results representative of
829 three independent experiments are shown.

830

831 **Fig. 3.** The SAPK pathway negatively regulates hyphal growth in *S. japonicus*.

832 (A) Cells ($\sim 10^6$) of wild type, *sty1* Δ , *atf1* Δ and *pyp1* Δ strains were spotted on YES plates, incubated for 2 days
833 at 30°C, and photographed before and after washing extensively (30 sec) with distilled water. Results
834 representative of three independent experiments are shown. (B) Cells of the above strains were grown in YES
835 plates for 12 h at 30°C, recovered by extensive washing with YES medium, and observed by phase-contrast
836 microscopy. Quantification (expressed as percentage) of yeasts (Y), vacuolated yeasts (V), transition forms
837 (T) and hyphae (H) present in each culture is shown in the left panel. Percentages are expressed as mean \pm SD
838 and correspond to biological triplicates ($n \geq 200$ cells/sample). *, $P < 0.05$; **, $P < 0.005$; ****, $P < 0.0001$, as
839 calculated by unpaired Student's *t* test. Representative phase-contrast micrographs different cell morphologies
840 found for each strain are shown in the right panel. Scale bar: 10 μ m. (C) Cell length represented as box and
841 whisker plots in *S. japonicus* wild type, *sty1* Δ *atf1* Δ , and *pyp1* Δ mutants growing exponentially in high
842 glucose (6%) YES medium for 6h in the absence or presence of 0.2 μ M CPT. Experiment was performed per
843 triplicate ($n \geq 200$ cells) and quantification of one is shown. ****, $P < 0.0001$, as calculated by unpaired
844 Student's *t* test. (D) Wild type *S. japonicus* strain growing exponentially (10^6 cells/ml) in high glucose (6%)
845 YES medium remained untreated (DMSO; negative control) or treated with 0.2 μ M CPT for the indicated
846 times. Activated/total Sty1 were detected with anti-phospho-p38 and anti-Hog1 antibodies, respectively. Anti-
847 cdc2 was used as loading control. Relative units as mean \pm SD (biological triplicates) for Sty1
848 phosphorylation (dark grey bars) and total Sty1 levels (light grey bars) were determined with respect to the

849 internal control (anti-cdc2 blot). (E) Wild type, *sty1Δ*, *atf1Δ*, and *pyp1Δ* strains were grown in high glucose
850 (6%) YES medium with 0.2 μM CPT for 24h, and the percentage of filaments/hyphae (dark grey bars) and
851 branched filaments/hyphae (light grey bars) were quantified. Percentages are expressed as mean ± SD and
852 correspond to biological triplicates (n≥200 cells/sample). **, P<0.005; ***, P<0.001; ****, P<0.0001, as
853 calculated by unpaired Student's *t* test. The right panels show the representative cell morphology of each
854 strain observed by fluorescence microscopy after staining with calcofluor white. Scale bar: 10 μm. (F) Cells
855 from log-phase cultures of the indicated strains growing in YES medium (2.10⁶) were spotted on YEMA
856 plates, incubated at 30°C for 7 days, and then photographed. The total area of mycelial expansion (expressed
857 as relative units) was measured for each strain (n≥6) and represented as scatter plot. **, P<0.005; ****,
858 P<0.001; ns, not significant, as calculated by unpaired Student's *t* test. (G) Exponentially growing *S.*
859 *japonicus* wild type cells were inoculated at an initial cell density of 10⁶ cells/ml in high glucose (6%) YES
860 medium and incubated for 6h with 0.2 μM CPT without further treatment or supplemented with 0.3 M KCl,
861 Cell length is represented as box and whisker plots. Data obtained after quantification of one experiment
862 performed per triplicate (n≥ 200 cells/sample) is shown. ****, P<0.0001, as calculated by unpaired Student's
863 *t* test. (H) Cells from a log-phase culture of wild type strain growing in YES medium (2.10⁶) were spotted on
864 YEMA and YEMA+0.6 M KCl plates, incubated at 30°C for 7 days, and then photographed. The total area of
865 mycelial expansion was measured (n≥6) and represented as scatter plot. ****, P<0.001, as calculated by
866 unpaired Student's *t* test.

867

868 **Fig. 4.** *S. japonicus* QS is partially suppressed in the absence of SAPK function.

869 (A) Exponentially growing *S. japonicus* wild type, *sty1Δ*, and *atf1Δ* cells were inoculated at the initial cell
870 densities of 5.10⁵, 5.10⁶, or 5.10⁷ cells/ml in high glucose (6%) YES medium, and incubated for 6h in the
871 absence or presence of 0.2 μM CPT. Cell length is represented as box and whisker plots. Data obtained after
872 quantification of one experiment performed per triplicate (n≥ 200 cells/strain) is shown. ****, P<0.0001; ns,
873 not significant, as calculated by unpaired Student's *t* test. (B) Media supernatants were recovered by filter-
874 sterilization of stationary phase cultures of wild type, *sty1Δ*, and *atf1Δ* strains, and the concentration of
875 phenylethanol (grey bars) and tryptophol (black bars) secreted into the medium was determined by GC/MS or
876 HPLC/MS analysis. Data are expressed as mean ± SD and correspond to biological triplicates. (C) Cell length

877 represented as box and whisker plots in *S. japonicus* wild type, *sty1Δ*, and *atf1Δ* strains cells growing
878 exponentially for 6h in the presence of 0.2 μM CPT in either unconditioned or conditioned YES medium (3%
879 glucose) obtained from a culture of the wild type strain growing to a density of 5.10⁶, 5.10⁷, or 10⁸ cells/ml.
880 The experiment was performed per triplicate (n ≥ 200 cells) and quantification of one is shown. ****,
881 $P < 0.0001$, as calculated by unpaired Student's *t* test. (D) Wild type *S. japonicus* strain growing exponentially
882 (10⁶ cells/ml) in high glucose (6%) YES medium remained untreated (DMSO; negative control) or treated
883 with 1, 2, 5 or 10 mM phenylethanol for 60 minutes. Activated Sty1 was detected with anti-phospho-p38, while
884 anti-cdc2 was used as loading control. Relative Sty1 activation units as mean ± SD (biological triplicates)
885 were determined with respect to the internal control (anti-cdc2 blot).

886

887 **Fig. 5.** Nrg1 activates hyphal growth in *S. japonicus* and is repressed by QS and the SAPK pathway.

888 (A) Venn diagrams indicating the number of differentially expressed up- and downregulated genes during
889 unperturbed growth in *sty1Δ* and *atf1Δ* mutants with respect to wild type cells. (B) Heatmap of the subset of
890 differentially expressed genes (up- and downregulated) during unperturbed growth in *sty1Δ* and *atf1Δ* mutants
891 with respect to wild type cells. Green indicates decrease and red indicates increase in gene expression. (C)
892 *nrg1*⁺ mRNA levels were measured by qPCR from total RNA extracted from cell samples corresponding to *S.*
893 *japonicus* wild type, *sty1Δ*, *atf1Δ*, *pyp1Δ*, and *pka1Δ* strains growing exponentially in YES medium. Results
894 are shown as relative fold expression (mean ± SD) from three biological repeats. **, $P < 0.005$; ns, not
895 significant, as calculated by unpaired Student's *t* test. (D) *nrg1*⁺ mRNA levels measured by qPCR from total
896 RNA extracted from cell samples from wild type, *sty1Δ* and *atf1Δ* strains growing exponentially (time 0h),
897 incubated for 3h in the presence of 0.2 μM CPT, or for 3h in the presence of 0.2 μM CPT plus 0.5 mM
898 phenylethanol (PE). Results are shown as relative fold expression (mean ± SD) from three biological repeats.
899 *, $P < 0.05$; **, $P < 0.005$; as calculated by unpaired Student's *t* test. (E) Cell length represented as box and
900 whisker plots in *S. japonicus* wild type, and *nrg1Δ* mutants growing exponentially in high glucose (6%) YES
901 medium for 6h in the presence of 0.2 μM CPT. Experiment was performed per triplicate (n ≥ 300 cells) and
902 quantification of one is shown. ****, $P < 0.0001$, as calculated by unpaired Student's *t* test. (F) Cells from log-
903 phase cultures of the indicated strains growing in YES medium (2.10⁶) were spotted on YEMA plates,
904 incubated at 30°C for 7 days, and then photographed. The total area of mycelial expansion (expressed as

905 relative units) was measured for each strain ($n \geq 6$) and is represented as scatter plot. *, $P < 0.05$; **, $P < 0.005$;
906 ***, $P < 0.001$; as calculated by unpaired Student's t test.

907

908

909

910 **Supplementary figure legends**

911 **Figure S1.** (A) Detection of phenylethanol by GC/MS analysis. Upper panel shows a typical gas
912 chromatogram of an extracted sample from conditioned medium. Lower panel shows the mass spectra
913 correspondent to peak visible at a ~9.1 min retention time that is identified as phenylethanol by the presence
914 of the characteristic ion of m/z 91. (B) Detection of tryptophol by HPLC/MS analysis. Upper panel shows a
915 liquid chromatogram of an extracted sample from conditioned medium. Lower panel: tryptophol was detected
916 as the peak with a ~4.3 min retention time by the characteristic ion of m/z 162.09.

917

918 **Figure S2.** Growth curves of *S. japonicus* wild type strain in YES medium (6% glucose) supplemented with
919 the indicated amounts of phenylethanol, tryptophol and tyrosol.

920

921 **Figure S3.** (A) ClustalW analysis of amino-acids sequences of Sty1 MAPKs in *S. pombe* and *S. japonicus*.
922 The analysis was performed on the genome.jp server (<https://www.genome.jp/tools-bin/clustalw>) using the
923 default settings. Identical amino-acids are marked with * and shaded in blue. Conserved residues/motifs
924 involved in ATP binding are shaded in yellow. Putative MAPKK (-DXXD- motif) and common (-ED- motif)
925 docking sites are shaded in purple. The conserved -TGY- activation loop specific of MAP kinases of the p38
926 type is shaded in green. (B) Anti-Hog1 and phospho-p38 antibodies specifically detect the respective total
927 and dually phosphorylated isoforms of Sty1 in total extracts from *S. japonicus* wild type cells, but not in the
928 *sty1Δ* mutant (C) Anti-Hog1 and phospho-p38 antibodies were employed to detect the respective total and
929 dually phosphorylated isoforms of Sty1 in samples from wild type *S. japonicus* cells growing in YES medium
930 at the indicated cellular densities. (D) ClustalW analysis of amino-acids sequences of Atf1 transcription factor
931 in *S. pombe* and *S. japonicus*. Identical amino-acids are marked with * and shaded in blue. The conserved
932 HRA (recombination), osmotic stress response, and basic-leucine zipper (DNA binding) domains are shown.
933 Putative MAPK-dependent phosphorylation sites (SP/TP) present in both proteins are underlined.

934

935 **Figure S4.** (A) Upper panel. *S. japonicus* wild type and *sty1Δ* strains were grown in YES medium. Samples
936 were taken at the indicated times (days), incubated with phloxine B, and the percentage of viable (non-

937 stained) cells was determined microscopically. Results from an experiment performed per triplicate are
938 shown. Lower panel. Serially diluted cells from samples described above were spotted on YES solid plates,
939 incubated for 3 days at 30°C, and photographed. Results representative of three independent experiments are
940 shown. (B) Serially diluted cells of wild type, *sty1Δ*, *atf1Δ* and *pyp1Δ* strains were spotted on YES plates
941 supplemented with or without 0.2 μM CPT and incubated for 3 days at 30°C. Results representative of three
942 independent experiments are shown.

943

944 **Figure S5.** mRNA levels of selected up- and down-regulated genes identified in RNAseq experiments were
945 measured by qPCR from total RNA extracted from cell samples corresponding to *S. japonicus* wild type,
946 *sty1Δ*, and *atf1Δ* strains growing exponentially in YES medium. Results are shown as relative fold expression
947 (mean ± SD) from three biological repeats. *, $P < 0.05$; **, $P < 0.005$; ***, $P < 0.001$, as calculated by unpaired
948 Student's *t* test.

949

950 **Figure S6.** Frequency of GO terms for common up-regulated (A) and down-regulated (B) genes in *sty1Δ* and
951 *atf1Δ* mutants.

952

953 **Figure S7.** ClustalW analysis of amino-acids sequences of Nrg1 transcription factor in *S. pombe* and *S.*
954 *japonicus*. The analysis was performed on the genome.jp server (<https://www.genome.jp/tools-bin/clustalw>)
955 using the default settings. Identical amino-acids are marked with * and shaded in blue. The putative C₂H₂ zinc
956 finger region and the conserved cysteine and histidine residues are marked with a black line and shaded in red,
957 respectively. The putative MAPK consensus phosphorylation sites are shown underlined.

958

959 **Figure S8.** (A) Exponentially growing *S. japonicus* wild type cells were inoculated at an initial cell density of
960 10⁶ cells/ml in high glucose (6%) YES medium and incubated for 6h with 0.2 μM CPT without further
961 treatment (untreated) or in the presence of the indicated amounts of farnesol. Cell length is represented as box
962 and whisker plots. Data obtained after quantification of one experiment performed per triplicate (n ≥ 200
963 cells/sample) is shown. ****, $P < 0.0001$, as calculated by unpaired Student's *t* test. (B) Cells from *S. japonicus*
964 wild type cells growing in YES medium (2.10⁶) were spotted on YEMA plates in the absence or presence of

965 40 μ M farnesol, incubated at 30°C for 7 days, and then photographed. The total area of mycelial expansion
966 (expressed as relative units) was measured ($n \geq 6$) and is represented as scatter plot. **, $P < 0.005$, as calculated
967 by unpaired Student's t test.

968

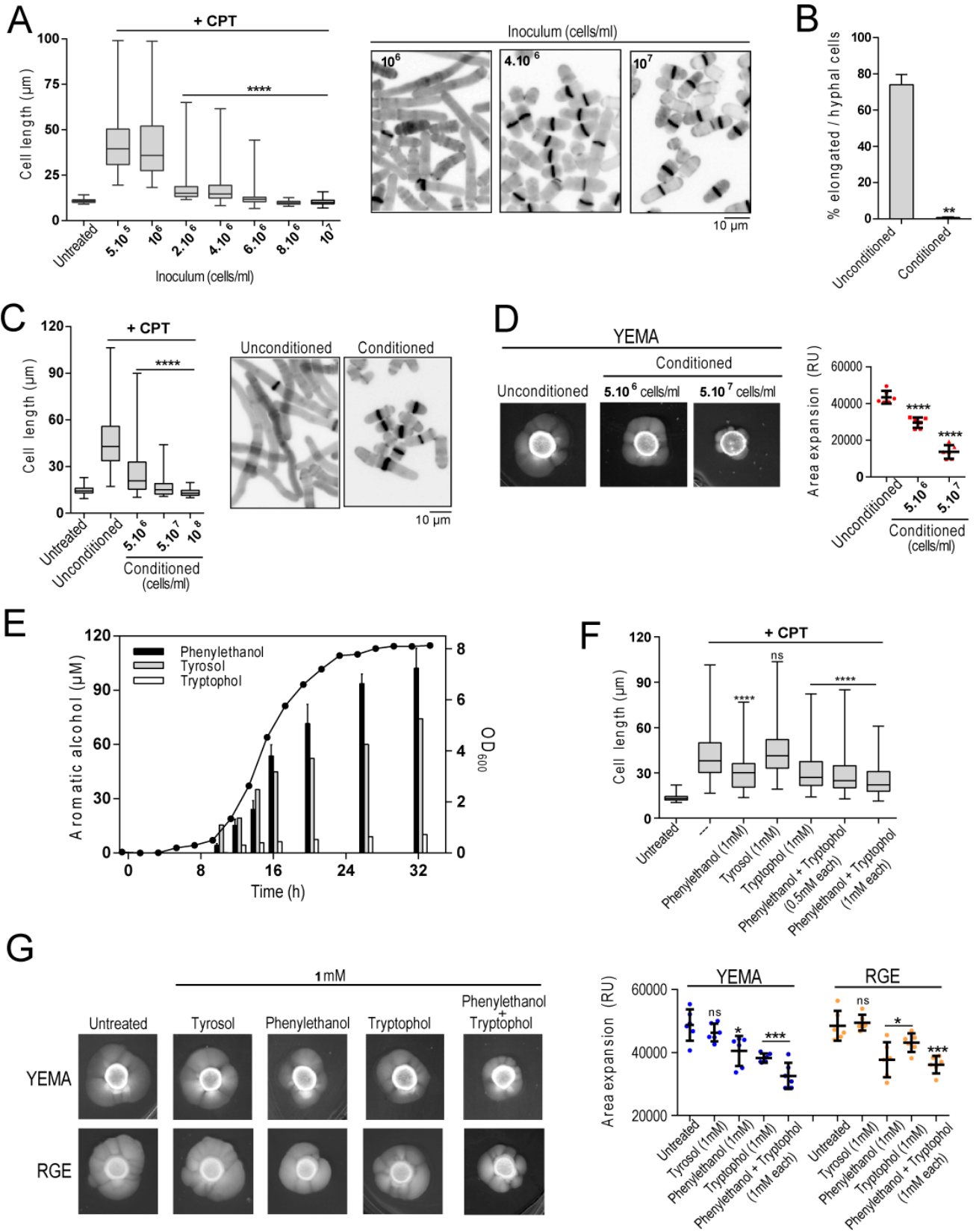


Fig 1

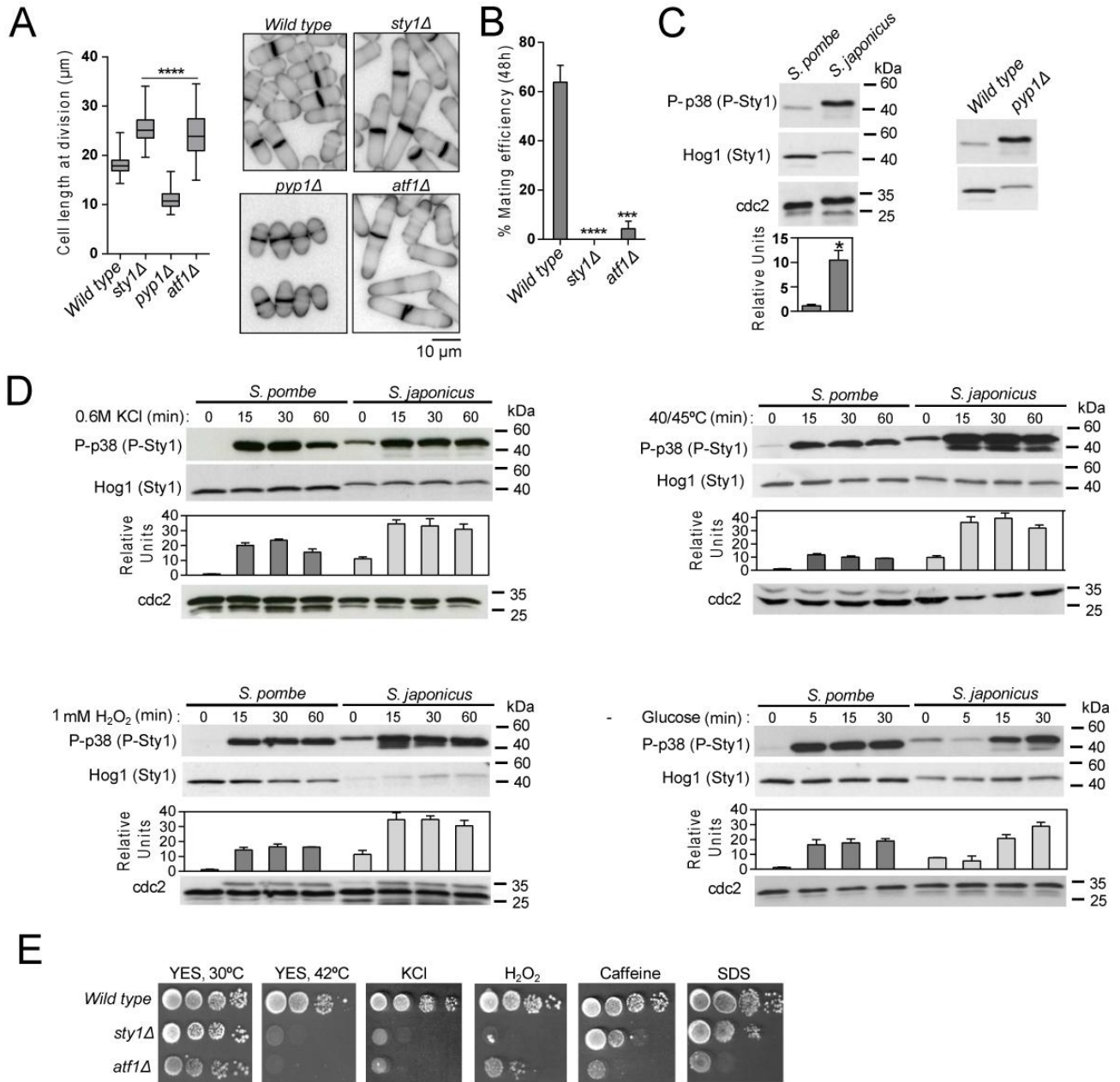


Fig 2

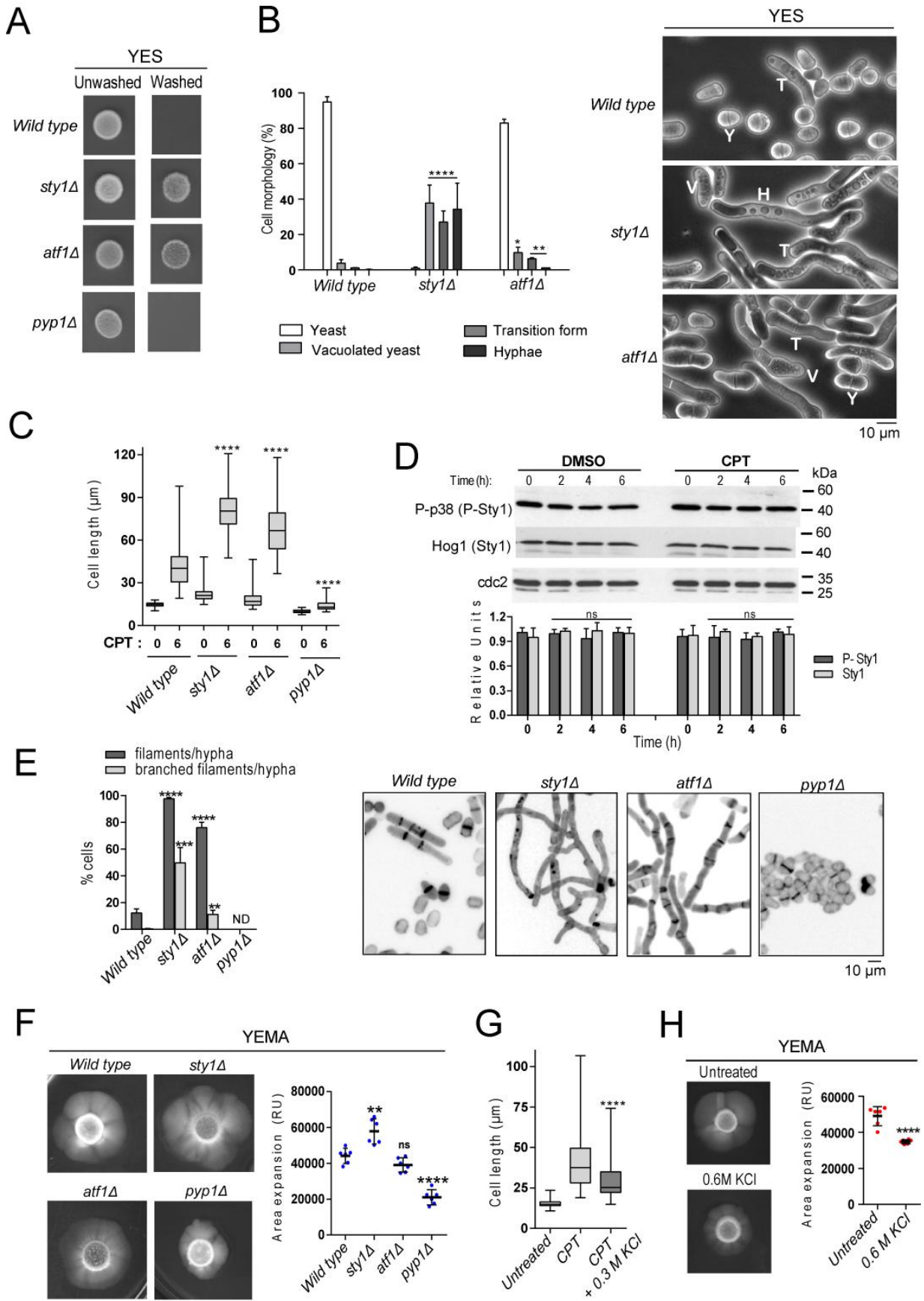
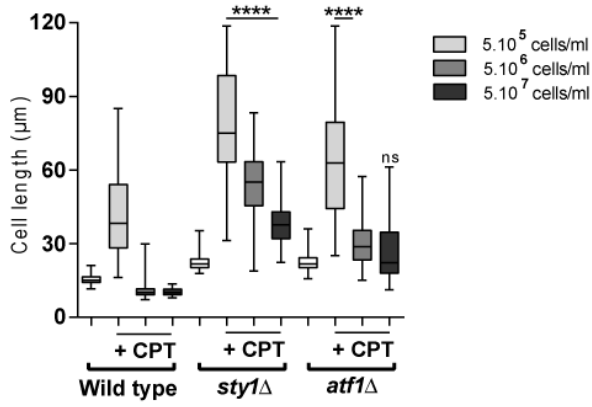
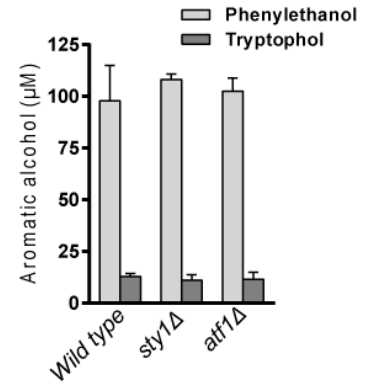


Fig 3

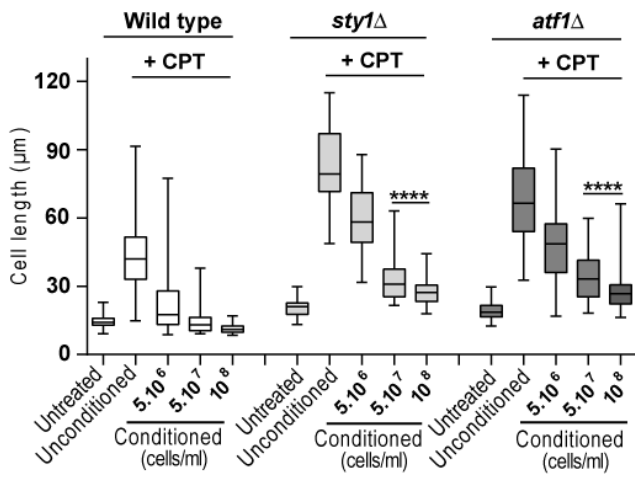
A



B



C



D

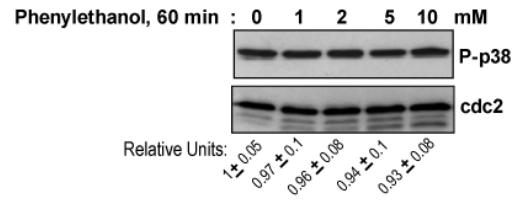


Fig 4

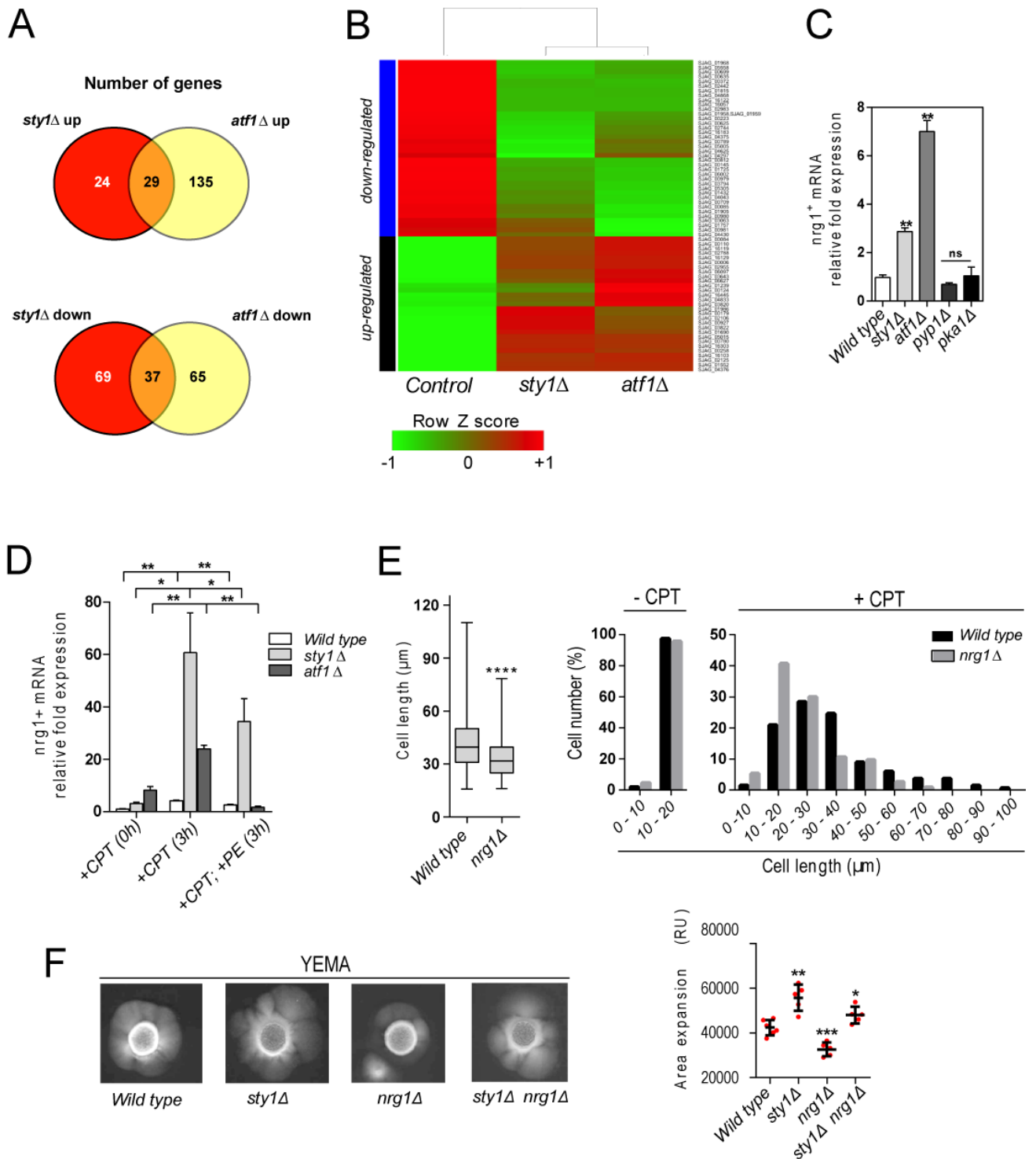


Fig 5

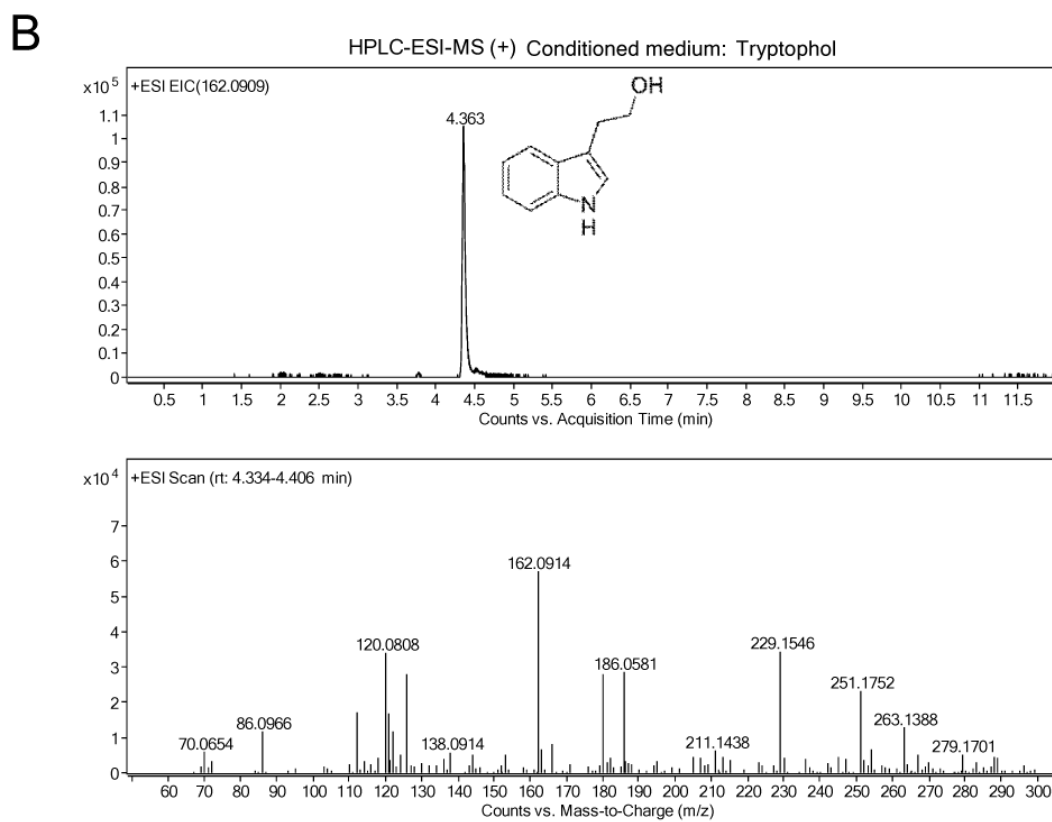
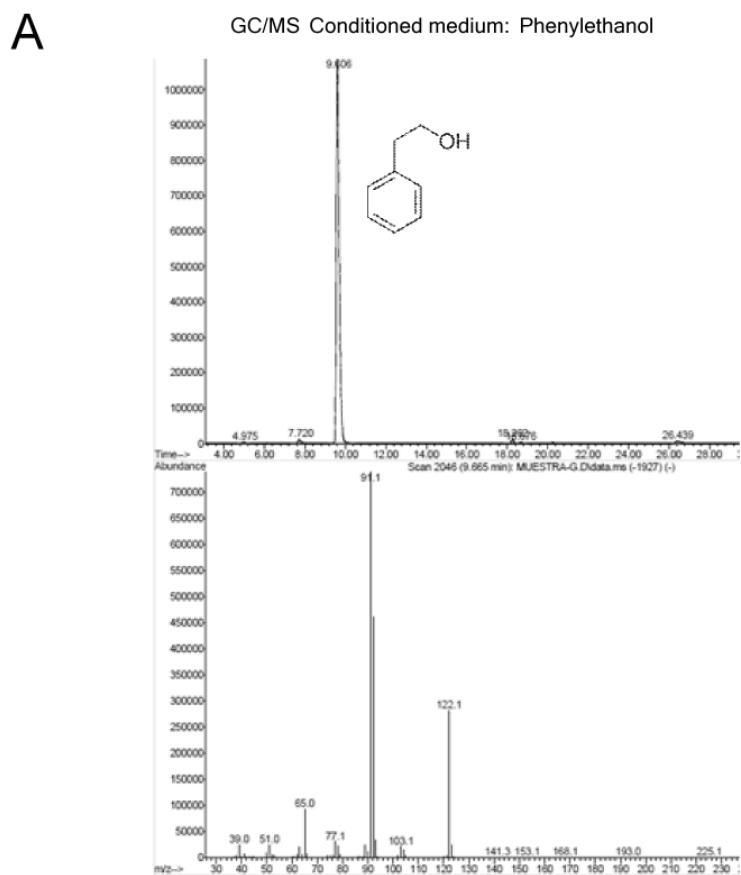


Fig S1

975

976

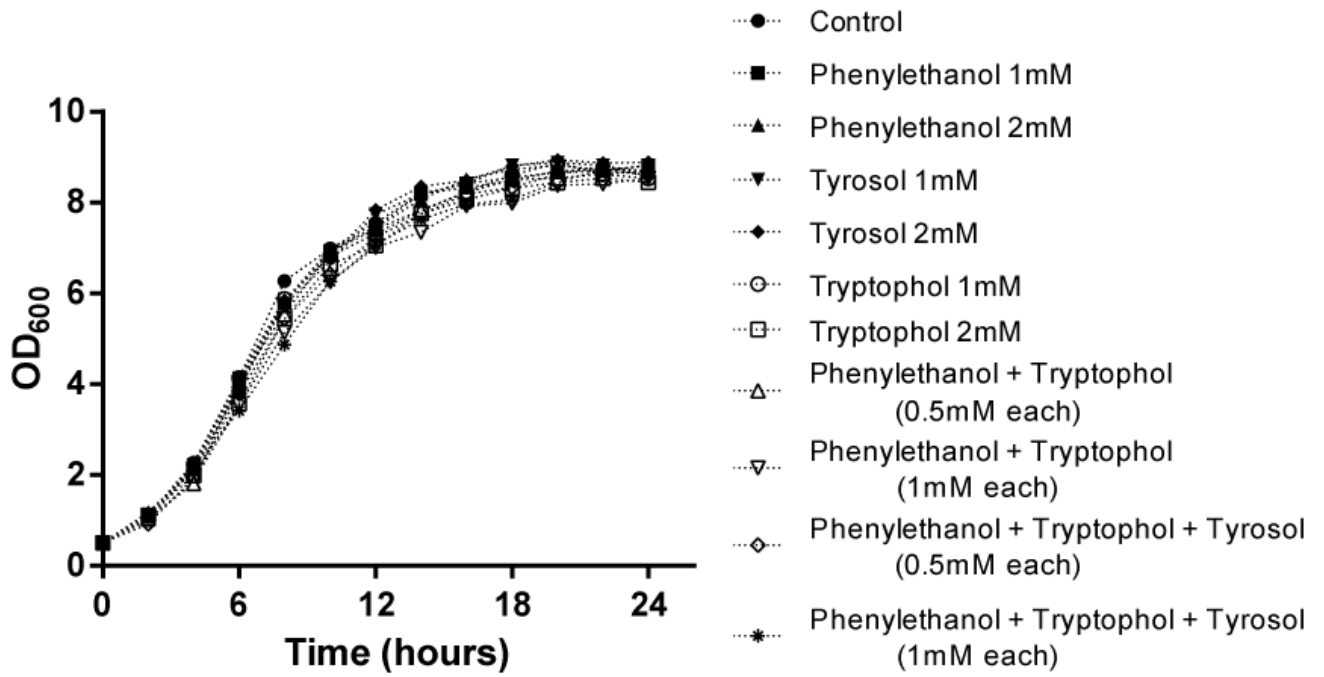
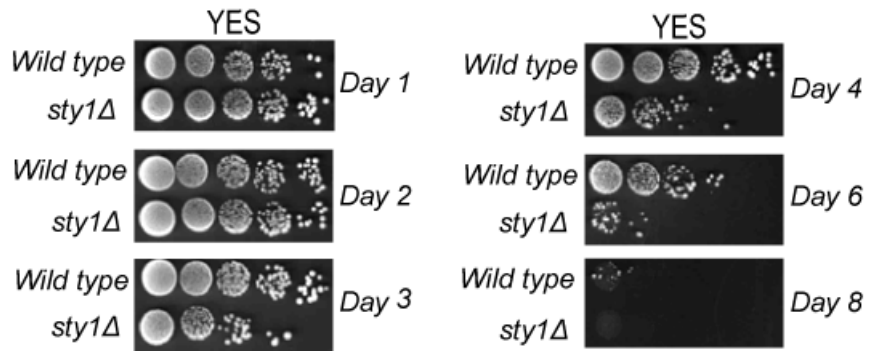
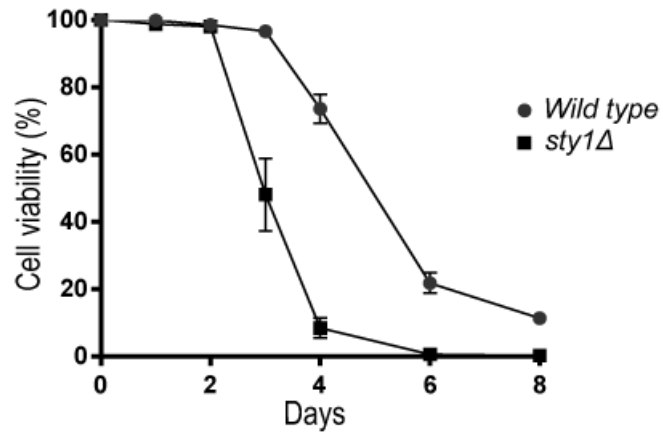


Fig S2

A



B

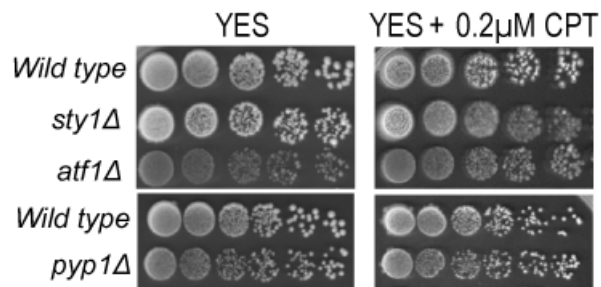
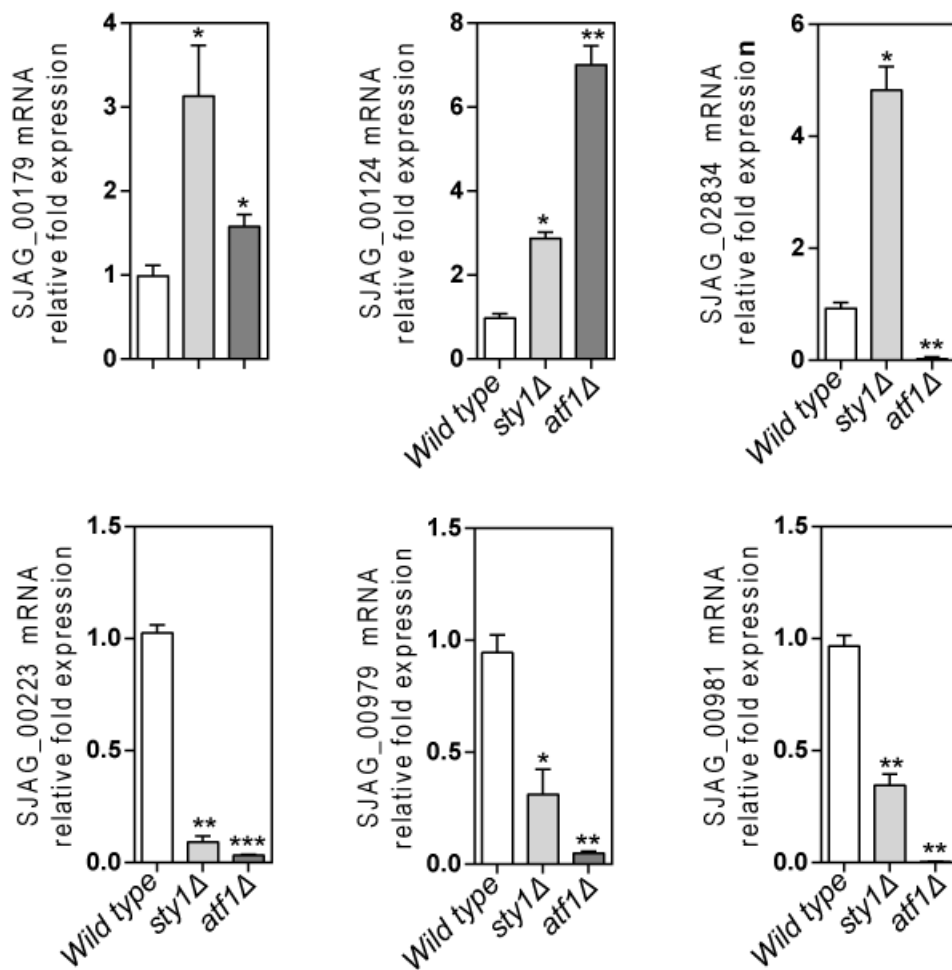


Fig S4



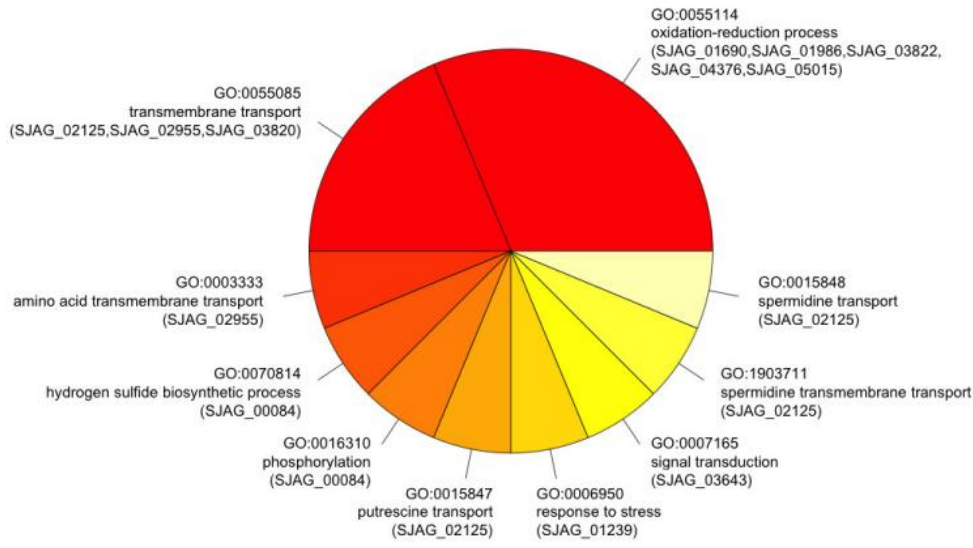
Gene	Function	Up-regulated in <i>sty1Δ</i> and <i>atf1Δ</i> cells	Down-regulated in <i>sty1Δ</i> and <i>atf1Δ</i> cells
SJAG_00179	Glutathione S-transferase	+/+	
SJAG_00124	Transcriptional regulator Nrg1	+/+	
SJAG_00223	Hsp9-like protein		+/+
SJAG_00979	Transcription factor Atf31		+/+
SJAG_00981	Fungal cellulose binding domain-containing protein		+/+
SJAG_02834	Siderophore iron transporter 1	+/-	-/+

Fig S5

980
981

A

Frequency of GO terms for common upregulated genes in *sty1Δ* and *atf1Δ* cells



B

Frequency of GO terms for common downregulated genes in *sty1Δ* and *atf1Δ* cells

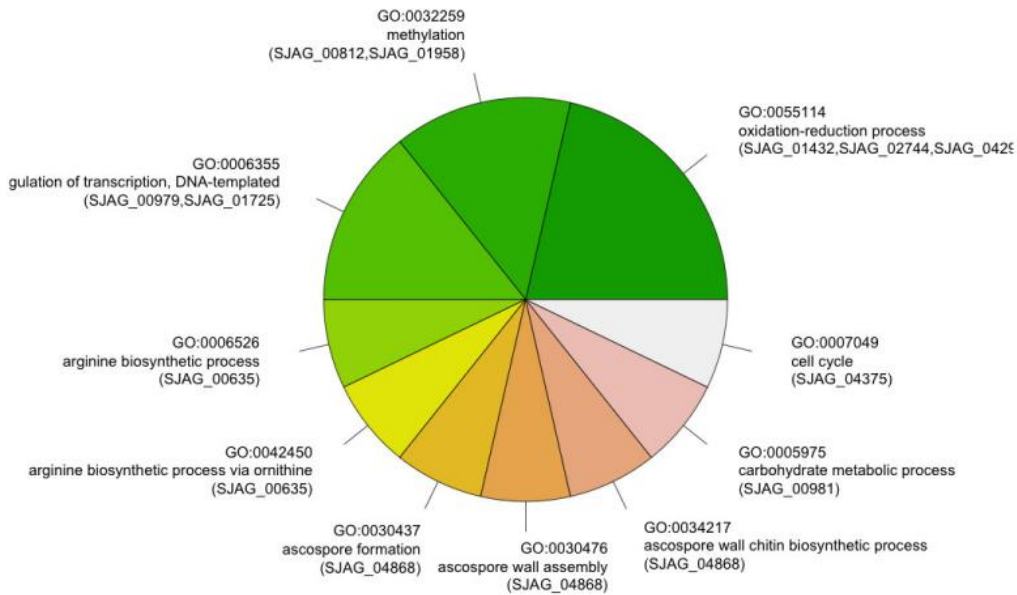


Fig S6

Nrg1

```

S.japonicus -----MSASLCVTTATC-----
C.albicans  MLYQQSYPIITNKLLNASAAAGSTSTASIIDGGCTLSKPGSGKTKSTTSLPSFNELLTSLIPL
              : . * . : .*

S.japonicus -----QRVSILSDTPWDD-----PRFVVPPFISSMPSVTSAPVVSVSAD
C.albicans  PNEFKPSTNNTNQAAAAATATSPYNYMGPPAQHRLPTPPYPMSPTTATAATPLSQQSP
              * . : : : * : * * * : . : * . * * : . :

S.japonicus MPKPTTIYRSRIPLG-----LLTDEMPPLTPIMPASS-----
C.albicans  HLQFQQTQQPQPYHQYYNYQYAAPPYPHLSQVPPASYYQQRHQQPMYQNTNGVPIIIR
              :* :. * : * * * : : * . : *

S.japonicus PTPPTTP-----AGECAGGPVRRKQRS AVRNTTKGKTYQHCGKTF TTS
C.albicans  PSPGLITPTSTTFDHAKIRSNSTGDLSANSLALSNNNTQSKDPRRKHVCKVCSRSE TTS
              * : * . * : * : : : : . . . . : * * : : * * * *

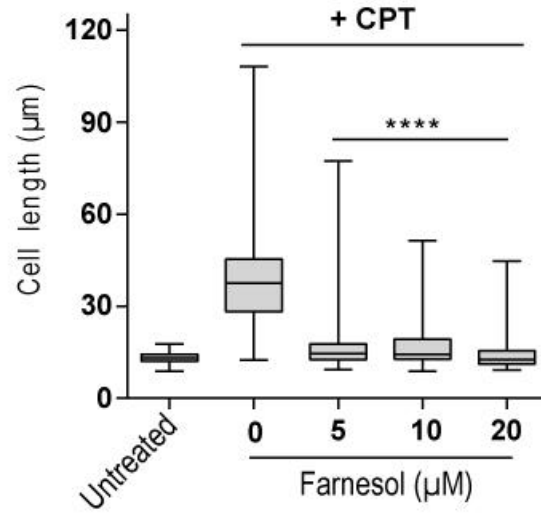
S.japonicus GHLARLNRIHMGEKNYEC--RICHSRFSRRDNCSDTRTFKQKPNVSLISSFAPIYLR
C.albicans  GHLARLNRIHTGERKHQCPWPTCEARFARQDNCNQH YKTH TNG-----K
              * * * * * * * * * * * * * * * * * * * * * * * * * * * * *

S.japonicus SPSNTSPFRD TVSSPRSCSSSPNSISSLLSS
C.albicans  NKRNRQQHRTLEASHVGTKYNTKSLV-----
              . * . . * : * . . . : * :

```

Fig S7

A



B

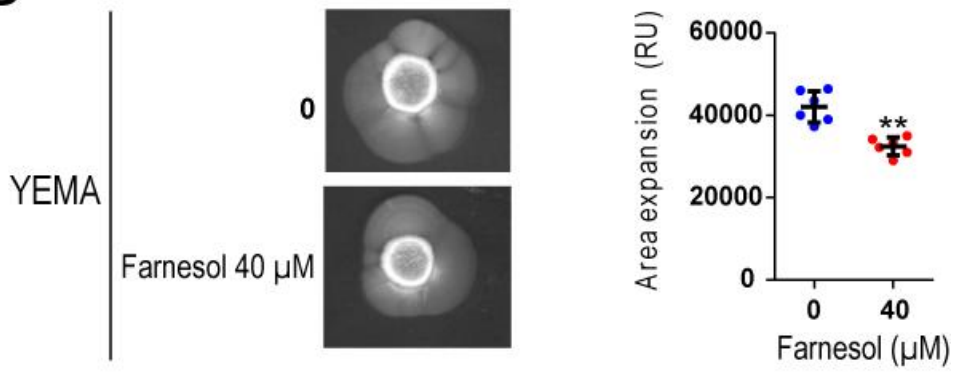


Fig S8

985

986 **Supplementary Tables**

987 **Table S1-S8.** Lists of up- and downregulated genes in exponentially growing *sty1* Δ and *atf1* Δ mutants

988 extracted from RNA seq data.

989 **Table S9.** Yeast strains used in this study

990 **Table S10.** Oligonucleotides

991

Table S9. *S. japonicus* and *S. pombe* strains used in this work.

<i>S. japonicus</i> strains	Genotype	Source
NIG2017	<i>h</i> ⁺	Furuya & Niki 2009
NIG5091	<i>h</i> ⁻ <i>ura4-D3</i>	Furuya & Niki 2009
NIG2028	<i>h</i> ⁻	Furuya & Niki 2009
TSJ101	<i>h</i> ⁻ <i>ura4-D3 sty1::ura4</i> ⁺	This work
TSJ105	<i>h</i> ⁻ <i>ura4-D3 atf1::ura4</i> ⁺	This work
TSJ106	<i>h</i> ⁻ <i>ura4-D3 nrg1::ura4</i> ⁺	This work
TSJ108	<i>h</i> ⁻ <i>ura4-D3 nrg1::ura4</i> ⁺ <i>sty1::NatMX6</i>	This work
TSJ109	<i>h</i> ⁻ <i>ura4-D3 pyp1::ura4</i> ⁺	This work
TSJ110	<i>h</i> ⁻ <i>ura4-D3 pka1::ura4</i> ⁺	This work
<i>S. pombe</i> strains	Genotype	Source
L972	<i>h</i> ⁻ <i>prototroph</i>	U. Leupold

992

993

994 **Table S10.** Oligonucleotides used in this work.
995

OLIGONUCLEOTIDE	SEQUENCE 5'-3'	Use
Leu1 FWD	GATGTCGGCGATGTGAATAAA	q-PCR
Leu1 REV	GGGAGGACGACAATCTTCTTA	q-PCR
Nrg1 (SJAG_00124) FWD	TAAGAACCAGAAGCCCAACT	q-PCR
Nrg1 (SJAG_00124) REV	AGGAGGACAATAGGGATGAAAT	q-PCR
Gst2 (SJAG_00179) FWD	CCTAACCCCTTGGAAGGTAGTT	q-PCR
Gst2 (SJAG_00179) REV	TGTTAGCGTGGTCCACTAAT	q-PCR
Hsp9 (SJAG_00223) FWD	AGTATGTCACTCCCGACTCCT	q-PCR
Hsp9 (SJAG_00223) REV	TCTGCTCGTCGCTCTTGAAG	q-PCR
Atf31 (SJAG_00979) FWD	TTGAACCCACAAGCAGAAAG	q-PCR
Atf31 (SJAG_00979) REV	TCTGGCTTTAGAATGGGAAGA	q-PCR
SJAG_00981 FWD	CTTCCGGTTCGAGTGTATAA	q-PCR
SJAG_00981 REV	CCTTCGGTACAACAAGTAGGA	q-PCR
SJAG_02834 FWD	GGTCACATAGCCAACACATAC	q-PCR
SJAG_02834 REV	TGTACCACGATAGCGAATCA	q-PCR
URA4-JP-COMP-R	CTTCTTGGCGACTGCATTAGGATGC	Common oligonucleotide for confirmation of <i>ura4⁺</i> deletions.
NAT-COMP-R	CTCATGTAGAGCGCCTGCCGC	Common oligonucleotide for confirmation of <i>NatR</i> deletions.
NRG1Djp-W2	AACCTAAACCTGACCGCAAAC	<i>nrg1⁺</i> deletion
NRG1Djp-X (URA4)	GAGCGGAAGAACGGAATCGTGCGGCCCGGTGCAGTCGCTTTAGC AGGGTGC	<i>nrg1⁺</i> deletion (<i>ura4⁺</i>)
NRG1Djp-Y (URA4)	GCAGTGCGGTATCGTATAATTAGTGTCCATAACTCTCGCTCGAGAGC CGCG	<i>nrg1⁺</i> deletion (<i>ura4⁺</i>)
NRG1Djp-Z2	TAGGAACAGATGAACTTGGCTCT	<i>nrg1⁺</i> deletion
NRG1Djp-COMP5'	CACTGCCTGTCTGCACGACAACCTG	Confirmation of <i>nrg1⁺</i> deletion.
STY1Djp-W	GCATGGGCGCGTTCCGGTCTTGTATG	<i>sty1⁺</i> deletion
STY1Djp-X (URA4)	GAGCGGAAGAACGGAATCGTGCGGCCACACCAGCACTGTGGACG TACTTC	<i>sty1⁺</i> deletion (<i>ura4⁺</i>)
STY1Djp-Y (URA4)	GCAGTGCGGTATCGTATAATTAGTGTGACGATCTGCAGCAAGAATAC ATTG	<i>sty1⁺</i> deletion (<i>ura4⁺</i>)
STY1Djp-Z	TGCTTGCACCTCACTATCCACATTATG	<i>sty1⁺</i> deletion
STY1Djp-X (NAT)	TTAATTAACCCGGGATCCGACACCAGCACTGTGGACGTACTTC	<i>sty1⁺</i> deletion (<i>NatR</i>)
STY1Djp-Y (NAT)	GTTTAAACGAGCTCGAATTCGACGATCTGCAGCAAGAATACATTG	<i>sty1⁺</i> deletion (<i>NatR</i>)
STY1Djp-COMP5'	ATGGCTGAATTTGTTCTGACACAGAT	Confirmation of <i>sty1⁺</i> deletion.
ATF1Djp-W	TGGTGAACCACGGTTTGATTACC	<i>atf1⁺</i> deletion
ATF1Djp-X (URA4)	GAGCGGAAGAAC GGAATCGTGCGGCCCGTTTGCTGAGGCAGAGGCTTC	<i>atf1⁺</i> deletion (<i>ura4⁺</i>)
ATF1Djp-Y (URA4)	GCAGTGCGGTATCGTATAATTAGTGTCAATGACAAATCGTGATGCGC AG	<i>atf1⁺</i> deletion (<i>ura4⁺</i>)
ATF1Djp-Z	TGAATGGCCTGCACTAAAGTGACG	<i>atf1⁺</i> deletion
ATF1Djp-COMP5'	GCTCTGCCCGATTCCCTCTTACG	Confirmation of <i>atf1⁺</i> deletion.
PYP1Djp-W	CACGTGGAACAGCTCGTATCTC	<i>pyp1⁺</i> deletion
PYP1Djp-X	GAGCGGAAGAACGGAATCGTGCGGCCCATCATCGCGTTAAAGTGT CCAGG	<i>pyp1⁺</i> deletion (<i>ura4⁺</i>)
PYP1Djp-Y	GCAGTGCGGTATCGTATAATTAGTGTGACTTTGTCAGGATGATTCTC TCG	<i>pyp1⁺</i> deletion (<i>ura4⁺</i>)
PYP1Djp-Z	AACGAAAAGACGCACAAGTCACTGC	<i>pyp1⁺</i> deletion
PYPDjp-COMP5'	GGCCTATTTAAAGGTAGTCTACCACC	Confirmation of <i>pyp1⁺</i> deletion.
PKA1Djp-W	TGTTTAGTGCGTAGAGGAAGTCAAG	<i>pka1⁺</i> deletion

PKA1Djp-X (URA4)	GAGCGGAAGAACGGAATCGTGGCGGCCCTCCGTATCGGTTGATTT GGAAC	<i>pka1⁺</i> deletion (<i>ura4⁺</i>)
PKA1Djp-Y (URA4)	GCAGTGCGGTATCGTATAATTAGTGTTATCAACTGGGAATCTATCCT TAC	<i>pka1⁺</i> deletion (<i>ura4⁺</i>)
PKA1Djp-Z	AATGTACCCGCTATCTCAAACGCTGC	<i>pka1⁺</i> deletion
PKA1Djp-COMP5'	CTGCTGCATGTATGACGTTTGAGAAC	Confirmation of <i>pka1⁺</i> deletion.

996

997

S1 Table. sty1Δ up-regulated genes

Gene	STY1_mean	CONTROL_me	log2FC	Description
SJAG_00006	2,828265	1,0102715	1,48517425	hypothetical protein
SJAG_00084	366,671	166,756	1,1367475	adenylyl-sulfate kinase
SJAG_00110	7,22275	2,445735	1,56228014	But2 family protein
SJAG_00124	1,66348	0,571147	1,54227051	transcriptional regulator NRG1
SJAG_00179	382,0535	20,78725	4,20000386	glutathione S-transferase Gst2
SJAG_00257	81,33485	26,4993	1,61791939	hypothetical protein
SJAG_00258	2,58856	1,168465	1,14753524	hypothetical protein
SJAG_00780	8,07228	3,74854	1,10664742	hypothetical protein
SJAG_00927	4,638925	1,62873	1,51004306	hypothetical protein
SJAG_01239	53,99655	25,8489	1,06276434	protein phosphatase Fmp31
SJAG_01416	102,9918	45,6613	1,17348564	pig-L
SJAG_01552	1,30329	0,262511	2,31170836	hypothetical protein
SJAG_01690	25,12765	2,77317	3,17966779	NADP-dependent L-serine/L-allo-threonine dehydrogenase ydfG
SJAG_01986	282,2025	31,3656	3,1694757	alcohol dehydrogenase
SJAG_02076	24,68605	10,296	1,26161205	hypothetical protein
SJAG_02106	32,4933	9,72536	1,74031871	hypothetical protein
SJAG_02125	1,43034	0,3757585	1,92848048	urea transporter
SJAG_02788	8,671825	3,759075	1,20595794	fungal protein
SJAG_02812	2112,84	992,902	1,08946028	translation elongation factor eIF5A
SJAG_02834	48,4188	10,446155	2,21259531	siderophore iron transporter 1
SJAG_02928	5,475095	2,62326	1,06152319	hypothetical protein
SJAG_02955	9,830835	2,923165	1,74978269	general amino acid permease AGP2
SJAG_03475	827,443	306,516	1,43269755	sulfate adenylyltransferase
SJAG_03492	152,82	28,58845	2,41832906	NADP-dependent L-serine/L-allo-threonine dehydrogenase ydfG
SJAG_03494	310,1275	154,196	1,00809612	glutamate-cysteine ligase regulatory subunit
SJAG_03643	39,9933	18,15125	1,13968942	arrestin Aly1
SJAG_03759	166,094	76,68555	1,1149733	phosphoglycerate mutase
SJAG_03820	1,533005	0,6743025	1,18489455	hexose transporter Ght8
SJAG_03821	62,91495	11,698135	2,42712433	hypothetical protein
SJAG_03822	2,992785	0,3968775	2,91472296	alcohol dehydrogenase Adh4
SJAG_03961	237,067	118,08965	1,00541233	5-aminolevulinate synthase
SJAG_04124	66,65625	33,2334	1,00410626	DUF1776 family protein

S1 Table. sty1Δ up-regulated genes

SJAG_04269	4,114675	1,878215	1,13141626	hypothetical protein
SJAG_04365	11,09255	5,15836	1,10460669	hypothetical protein
SJAG_04376	1,356375	0,239964	2,49886621	peptidase
SJAG_04743	338,644	168,974	1,00296816	ferric reductase transmembrane component
SJAG_04833	1,768965	0,5627125	1,65243559	hypothetical protein
SJAG_05015	173,3225	73,83375	1,23110661	NADPH dehydrogenase
SJAG_05173	1,091205	0,272538	2,00139286	hypothetical protein
SJAG_06097	95,57135	12,44505	2,94100617	hypothetical protein
SJAG_06596	58,5555	27,9081	1,06912078	hypothetical protein
SJAG_06627	3,01731	1,146061	1,39657909	hypothetical protein
SJAG_16028	34,78845	9,8846	1,81535391	n/a
SJAG_16042	36,4151	0,5	6,1864649	n/a
SJAG_16075	151,8425	45,91295	1,72560261	n/a
SJAG_16103	13,7006	0,5	4,77616717	n/a
SJAG_16118	68,82765	31,54525	1,12556547	n/a
SJAG_16119	7,6375	0,5	3,93310047	n/a
SJAG_16127	45,75075	16,9944	1,42873597	n/a
SJAG_16129	7,5881	0,5	3,92373869	n/a
SJAG_16303	10,0963	0,5	4,33575478	n/a
SJAG_16443	42,96995	12,0673	1,83222518	n/a
SJAG_16445	26,1039	12,46605	1,06626096	n/a

S2 Table. sty1Δ down-regulated genes

Gene	STY1_mean	CONTROL_me	log2FC	Description
SJAG_00085	33,5832	93,55445	-1,47806657	DUF423 protein
SJAG_00097	0,8823105	3,21019	-1,86330033	5-aminolevulinate synthase
SJAG_00099	8,79049	24,04305	-1,45160443	Delta(12) fatty acid desaturase
SJAG_00138	8,03058	36,25915	-2,17476901	fungal protein
SJAG_00145	15,8531	44,5811	-1,49166723	RNA-binding protein
SJAG_00223	48,6741	929,2205	-4,25479477	hsp9-like protein
SJAG_00260	2,68744	7,657265	-1,51059664	succinate dehydrogenase iron-sulfur protein subunit
SJAG_00265	3,643795	10,015555	-1,45872867	D-arabinono-1,4-lactone oxidase
SJAG_00266	38,37745	95,6701	-1,31780925	transcription factor Atf1
SJAG_00372	156,1285	526,95	-1,75493216	plasma membrane proteolipid Pmp3
SJAG_00409	229,6135	468,7315	-1,02955428	glycerol-3-phosphate dehydrogenase Gpd1
SJAG_00449	8,891805	22,5877	-1,34498916	cytochrome C oxidase copper chaperone Cox17
SJAG_00452	29,10365	185,126	-2,66923553	ubiquitin
SJAG_00555	7,298095	16,41875	-1,16975246	zf-PARP type zinc finger protein
SJAG_00625	76,95695	214,6395	-1,47979207	hypothetical protein
SJAG_00635	7,916765	25,35125	-1,67907395	ornithine carbamoyltransferase Arg3
SJAG_00667	33,0519	81,79525	-1,30728386	endo-1,3-beta-glucanase Eng1
SJAG_00699	62,72575	145,7685	-1,21654927	tspO/peripheral benzodiazepine receptor
SJAG_00709	0,725534	1,94908	-1,42567818	hypothetical protein
SJAG_00788	1,18238	3,05638	-1,37013015	hypothetical protein
SJAG_00789	4,04648	64,51565	-3,9949098	hypothetical protein
SJAG_00812	90,649	187,0795	-1,04528847	phosphatidyl-N-methylethanolamine N-methyltransferase
SJAG_00979	0,559284	2,79279	-2,32005413	transcription factor atf31
SJAG_00980	0,481918	1,42571	-1,56482096	ATP-dependent DNA helicase Rdh54
SJAG_00981	14,18285	53,25545	-1,90878171	fungal cellulose binding domain-containing protein
SJAG_00993	15,34695	32,4833	-1,08174624	STE/STE7/MEK1 protein kinase Byr1
SJAG_01084	11,718	31,05845	-1,40625948	CAMK/CAMK1 protein kinase Srk1
SJAG_01427	8,280035	31,116	-1,90994784	alpha,alpha-trehalose-phosphate synthase
SJAG_01432	23,1352	46,4439	-1,00539955	hydroxyacid dehydrogenase
SJAG_01490	1,989295	6,141705	-1,62638198	ubiquinol-cytochrome-c reductase complex subunit 8
SJAG_01531	42,26305	105,29145	-1,3169195	alpha,alpha-trehalose-phosphate synthase
SJAG_01540	3,23956	6,63801	-1,03495292	Cullin 4

S2 Table. sty1Δ down-regulated genes

SJAG_01578	1,0064045	2,492915	-1,30862341	fungal protein
SJAG_01725	14,7266	57,46855	-1,96434826	transcription factor Atf21
SJAG_01757	0,463756	1,14554	-1,30458998	hypothetical protein
SJAG_01795	10,906255	25,53405	-1,22726659	hydrolase
SJAG_01815	10,44543	45,781	-2,13187709	hypothetical protein
SJAG_01869	15,6442	60,43445	-1,94974329	NADH/NADPH dependent indole-3-acetaldehyde reductase AKR3C2
SJAG_01905	2,58805	10,483995	-2,01825118	progesterone binding protein
SJAG_01968	128,5035	426,0035	-1,72905763	pepsin A
SJAG_02013	15,01195	52,2071	-1,79813463	tyrosine phosphatase Pyp1
SJAG_02122	1,80947	5,272385	-1,54288853	hypothetical protein
SJAG_02338	8,6195	24,4972	-1,50694077	non classical export pathway protein
SJAG_02432	85,245	214,9425	-1,33426365	vacuolar serine protease lsp6
SJAG_02442	11,92445	32,49385	-1,44624396	hypothetical protein
SJAG_02496	13,83025	52,88875	-1,93513364	D-amino acid oxidase
SJAG_02550	35,49925	71,71425	-1,01447127	DUF1941 family protein
SJAG_02569	2,09771	4,86485	-1,21358008	transcription factor
SJAG_02612	7,964325	18,86985	-1,24445896	fungal protein
SJAG_02626	88,75885	238,559	-1,42638323	protein kinase inhibitor
SJAG_02701	23,01955	50,6588	-1,13795327	bromodomain protein
SJAG_02744	15,508	85,72525	-2,46670757	cytochrome c
SJAG_02950	2,374475	7,339975	-1,62816658	galactokinase Gal1
SJAG_02951	2,412265	11,48828	-2,25170251	gal10
SJAG_02975	3,28861	7,20358	-1,13123614	hypoxia induced family protein
SJAG_02983	0,5	1,342175	-1,42457279	hypothetical protein
SJAG_02984	0,6448745	1,71266	-1,40914845	phosphoglycerate mutase family protein
SJAG_03063	47,9229	160,5175	-1,74394347	dienelactone hydrolase
SJAG_03201	2,70036	7,198125	-1,4144694	hypothetical protein
SJAG_03318	12,2909	24,67255	-1,00531627	N-acetyltransferase
SJAG_03388	18,3117	39,3405	-1,10324956	transcription factor Hsr1
SJAG_03603	38,1346	89,70465	-1,2340822	high-mobility group non-histone chromatin protein
SJAG_03606	4,75909	22,6118	-2,2483182	hexose transporter Ght6
SJAG_03786	426,936	1153,405	-1,43380746	aldehyde dehydrogenase
SJAG_03794	26,2432	52,5063	-1,00054689	DNAJ domain-containing protein Psi1

S2 Table. sty1Δ down-regulated genes

SJAG_03803	5,80574	13,00355	-1,16335367	hypothetical protein
SJAG_03804	8,008845	19,45315	-1,28033768	D-lactate dehydrogenase
SJAG_03818	0,588267	1,641725	-1,48066947	gal10
SJAG_03830	2,85949	18,212145	-2,67107109	hypothetical protein
SJAG_03958	7,90094	22,58115	-1,51502275	xylose and arabinose reductase
SJAG_04007	214,8525	774,7965	-1,85047087	fungal protein
SJAG_04008	7,278295	15,30665	-1,07248614	cytochrome c heme lyase
SJAG_04043	1,145435	16,41645	-3,84117469	hypothetical protein
SJAG_04055	132,8925	304,623	-1,19676519	heat shock protein S
SJAG_04135	1,690565	6,730355	-1,99317712	amino acid permease
SJAG_04227	9,251075	20,0122	-1,11318685	fungal protein
SJAG_04297	0,2512055	2,202005	-3,13187779	sulfonate dioxygenase
SJAG_04298	3,44859	21,84355	-2,66312882	hydantoin racemase family protein
SJAG_04299	0,190673	1,105964	-2,53613195	uricase
SJAG_04312	11,0821	25,6105	-1,20850413	AGC/PKA protein kinase Pka1
SJAG_04375	45,27445	156,9915	-1,79391743	septin Spn3
SJAG_04430	33,1786	70,6924	-1,09130211	hypothetical protein
SJAG_04458	2,66698	9,036025	-1,76048126	NAD binding dehydrogenase
SJAG_04568	1,154575	2,69024	-1,22037299	decaprenyl diphosphate synthase subunit Dps1
SJAG_04625	0,9118215	4,53031	-2,31278644	DUF1761 family protein
SJAG_04660	14,0903	29,39945	-1,06108684	xylose and arabinose reductase
SJAG_04662	1,698225	3,68487	-1,11758611	hypothetical protein
SJAG_04673	7,478895	21,97705	-1,55510071	thiamine transporter Thi9
SJAG_04682	8,80014	19,2508	-1,12932002	CCCH tandem zinc finger protein
SJAG_04711	18,9278	42,69435	-1,17353843	GTP cyclohydrolase II
SJAG_04713	12,0446	24,56965	-1,02849082	uracil phosphoribosyltransferase
SJAG_04789	1,192355	2,573135	-1,10971332	alpha-amylase Aah4
SJAG_04859	23,1768	63,57825	-1,45585192	alpha,alpha-trehalase Ntp1
SJAG_04868	1,2909	2,82928	-1,13205771	chitin synthase I
SJAG_05005	3,9484	13,89165	-1,81487791	fungal protein
SJAG_05181	24,6118	55,4105	-1,17080921	glutathione S-transferase Gst3
SJAG_05305	14,42907	53,44455	-1,88906452	membrane protein complex assembly protein
SJAG_05558	40,4894	91,0148	-1,1685569	fungal protein

S2 Table. sty1Δ down-regulated genes

SJAG_05896	1,846875	12,0208	-2,70237478	hypothetical protein
SJAG_06002	2,33124	9,252875	-1,98880416	hypothetical protein
SJAG_06111	0,357933	1,31765	-1,88020574	hypothetical protein
SJAG_16057	0,5	8,91508	-4,15624774	n/a
SJAG_16122	0,5	20,83475	-5,38091988	n/a
SJAG_16123	18,41485	37,4238	-1,02308641	n/a
SJAG_16142	0,5	19,4437	-5,28123087	n/a
SJAG_16183	11,58695	38,0743	-1,71631665	n/a

S3 Table. atf1Δ up-regulated genes

Gene	ATF1_mean	CONTROL_me	log2FC	Description
SJAG_00006	3,52446	1,0102715	1,80265918	hypothetical protein
SJAG_00026	2,218455	0,5596825	1,98687475	hypothetical protein
SJAG_00075	39,1397	13,81595	1,50229793	trichothecene 3-O-acetyltransferase
SJAG_00084	479,4945	166,756	1,5237756	adenylyl-sulfate kinase
SJAG_00091	43,2244	15,7396	1,45744706	fungal protein
SJAG_00097	15,22735	3,21019	2,2459343	5-aminolevulinate synthase
SJAG_00099	58,62485	24,04305	1,2858924	Delta(12) fatty acid desaturase
SJAG_00110	10,45211	2,445735	2,09545421	But2 family protein
SJAG_00121	44,57215	2,62936	4,08335897	hypothetical protein
SJAG_00124	23,6943	0,571147	5,37453412	transcriptional regulator NRG1
SJAG_00144	32,15515	15,1846	1,08244091	GRIP domain-containing protein
SJAG_00179	127,9507	20,78725	2,62181722	glutathione S-transferase Gst2
SJAG_00191	17,8584	6,109495	1,54747779	hypothetical protein
SJAG_00211	20,36705	10,15739	1,00370729	DUF803 domain-containing protein
SJAG_00237	18,19995	8,80279	1,04790173	hexitol dehydrogenase
SJAG_00238	1,42617	0,354537	2,00813786	glutathione S-transferase Gst1
SJAG_00240	4,04428	1,453455	1,47639648	alcohol dehydrogenase Adh4
SJAG_00242	337,2605	51,89395	2,7002251	hypothetical protein
SJAG_00258	2,35646	1,168465	1,01200667	hypothetical protein
SJAG_00358	15,3797	5,249965	1,55064765	tRNA(5-methylaminomethyl-2-thiouridylate)-methyltransferase
SJAG_00415	105,15965	33,7224	1,64080212	hypothetical protein
SJAG_00451	318,584	147,304	1,11287721	carboxypeptidase
SJAG_00528	2,839715	0,2986125	3,24939968	hypothetical protein
SJAG_00556	20,5942	7,48616	1,4599403	hypothetical protein
SJAG_00567	31,69675	13,29445	1,25351083	dymeclin 1
SJAG_00587	35,00715	0,518409	6,07741504	sphingoid long-chain base transporter RSB1
SJAG_00589	1,3611	0,538239	1,33845423	hypothetical protein
SJAG_00658	1616,32	420,4315	1,94277018	hypothetical protein
SJAG_00720	47,77305	20,3411	1,23179929	COP9/signalosome complex subunit Csn5
SJAG_00780	7,74405	3,74854	1,04675947	hypothetical protein
SJAG_00781	2,9274	1,0203895	1,52049993	P-factor pheromone Map2
SJAG_00788	10,336065	3,05638	1,75779122	hypothetical protein

S3 Table. atf1Δ up-regulated genes

SJAG_00804	13,24095	6,042075	1,13189064	SNARE Sft1
SJAG_00832	12,10435	3,880455	1,64122788	sulfatase modifying factor 1
SJAG_00927	3,357835	1,62873	1,04378388	hypothetical protein
SJAG_00963	4,003585	1,770175	1,17740044	HAL protein kinase Ppk8
SJAG_00976	18,0149	8,44574	1,0928949	cytochrome c oxidase subunit IV
SJAG_01007	38,9311	13,6062	1,51665891	nramp family manganese ion transporter
SJAG_01078	77,5771	18,2457	2,08807434	zinc homeostasis factor 1
SJAG_01130	53,8363	26,20115	1,03894913	hypothetical protein
SJAG_01168	53,5055	21,7217	1,30055018	membrane transporter
SJAG_01239	208,762	25,8489	3,01368434	protein phosphatase Fmp31
SJAG_01316	18,80215	6,42103	1,550021	hypothetical protein
SJAG_01346	70,62135	35,3004	1,00041987	hypothetical protein
SJAG_01372	160,385	60,0997	1,41610953	porphobilinogen synthase Hem2
SJAG_01437	158,7445	73,07695	1,11921828	synaptotagmin family C2 domain-containing protein
SJAG_01490	16,9497	6,141705	1,46454862	ubiquinol-cytochrome-c reductase complex subunit 8
SJAG_01505	2,83172	0,962165	1,55732239	acetate transporter
SJAG_01552	1,376025	0,262511	2,3900569	hypothetical protein
SJAG_01553	64,24945	6,28722	3,35318995	hypothetical protein
SJAG_01555	2,385185	0,384876	2,63163555	hypothetical protein
SJAG_01690	15,0661	2,77317	2,44169805	NADP-dependent L-serine/L-allo-threonine dehydrogenase ydfG
SJAG_01794	47,39245	22,8938	1,0497003	hypothetical protein
SJAG_01835	644,992	269,1125	1,26107186	1,3-beta-glucanosyltransferase Gas2
SJAG_01888	21,40515	10,5975	1,01423398	glucan 1,3-beta-glucosidase Exg2
SJAG_01919	109,405	11,7641	3,21721582	RNA-binding protein M
SJAG_01922	284,574	130,6165	1,1234667	citrate synthase Cit1
SJAG_01932	3,582	1,2158425	1,55880898	hypothetical protein
SJAG_01970	142,649	50,10715	1,50938125	thiamine-repressible acid phosphatase pho4
SJAG_01971	3,678785	1,274135	1,52971122	DNA-3-methyladenine glycosylase Mag1
SJAG_01975	85,19675	22,74925	1,90497941	kinetochore protein fta5
SJAG_01986	126,09425	31,3656	2,00724742	alcohol dehydrogenase
SJAG_02011	16,23465	6,60893	1,29658766	hypothetical protein
SJAG_02091	34,1475	6,51127	2,39076909	phospholipase B Plb1
SJAG_02106	22,11515	9,72536	1,18521147	hypothetical protein

S3 Table. atf1Δ up-regulated genes

SJAG_02113	2,42219	0,136585	4,14844108	amino acid permease
SJAG_02125	1,5768	0,3757585	2,06912204	urea transporter
SJAG_02148	15,5967	7,53826	1,04893735	glucose-6-phosphate 1-dehydrogenase
SJAG_02338	431,606	24,4972	4,13902616	non classical export pathway protein
SJAG_02339	49,7367	10,262295	2,27695739	RecA family ATPase Rlp1
SJAG_02344	57,10755	16,59905	1,78258082	spermine family transporter
SJAG_02350	3,404115	1,411325	1,27022953	fungal protein
SJAG_02567	81,39255	28,11675	1,5334669	phosphoprotein phosphatase
SJAG_02569	18,01355	4,86485	1,8886153	transcription factor
SJAG_02580	106,1455	29,4589	1,84926774	phosphoprotein phosphatase
SJAG_02665	53,65455	19,815	1,43710755	Vac7
SJAG_02735	1,0490945	0,2359565	2,15255182	siderophore iron transporter 1
SJAG_02785	62,02285	8,203305	2,91852265	protein kinase activator
SJAG_02788	10,9714	3,759075	1,54529803	fungal protein
SJAG_02794	84,2098	22,7356	1,88903506	cytochrome b5 reductase
SJAG_02925	56,11355	22,93625	1,29071965	hypothetical protein
SJAG_02941	11,552705	0,02960005	8,60841536	amino acid permease
SJAG_02946	12,14245	0,3109585	5,28719368	amino acid permease
SJAG_02950	15,5452	7,339975	1,08262212	galactokinase Gal1
SJAG_02955	12,6681	2,923165	2,11559699	general amino acid permease AGP2
SJAG_02963	46,6704	13,6811	1,7703236	NADP-dependent alcohol dehydrogenase
SJAG_02968	19,67215	4,56034	2,10894135	iron/zinc ion transporter
SJAG_02970	4,09503	1,25628	1,70471597	hypothetical protein
SJAG_02976	38,91575	9,70592	2,00341729	hypothetical protein
SJAG_03019	14,7853	4,85297	1,60722367	hypothetical protein
SJAG_03074	38,8345	14,58115	1,41323438	hypothetical protein
SJAG_03114	57,35875	27,7081	1,0497058	F1-ATPase delta subunit
SJAG_03204	29,98145	12,5273	1,25899465	phospholipase
SJAG_03221	100,9289	31,6753	1,67190915	Swi5 protein
SJAG_03244	352,0545	163,8685	1,10326023	bcap family protein
SJAG_03245	808,426	392,6545	1,04185529	RING finger-like protein Ini1
SJAG_03296	6,169375	0,7552015	3,03019081	inner membrane protein
SJAG_03297	2,3213	0,2212995	3,39086089	ribosomal protein subunit L19

S3 Table. atf1Δ up-regulated genes

SJAG_03303	2875,905	1131,475	1,34581131	manganese superoxide dismutase
SJAG_03304	46,36	12,03685	1,94542267	hypothetical protein
SJAG_03305	63,31895	24,8974	1,34664224	glycerol-3-phosphate O-acyltransferase
SJAG_03340	30,89875	7,856265	1,97563298	adaptor protein Ste4
SJAG_03361	591,3645	175,7075	1,75087187	rho GDP dissociation inhibitor Rdi1
SJAG_03493	10,5544	1,552435	2,7652398	peroxin Pex28/29
SJAG_03608	859,105	133,9883	2,68072744	hexose transporter Ght5
SJAG_03624	30,841	11,7394	1,39349087	phosphoric ester hydrolase Ssu72
SJAG_03643	55,77625	18,15125	1,61958204	arrestin Aly1
SJAG_03646	36,4625	13,58765	1,42411752	glucan 1,3-beta-glucosidase Exg3
SJAG_03647	28,72215	10,6076	1,43706547	MBF transcription factor complex subunit Rep1
SJAG_03735	47,51005	20,5794	1,2070318	transcription factor Esc1
SJAG_03766	14,02355	5,99919	1,22501198	hypothetical protein
SJAG_03778	2,36076	0,3692305	2,67665775	hypothetical protein
SJAG_03818	35,52125	1,641725	4,43539796	gal10
SJAG_03820	3,693395	0,6743025	2,45347971	hexose transporter Ght8
SJAG_03822	1,61908	0,3968775	2,02840859	alcohol dehydrogenase Adh4
SJAG_03824	5,118845	0,09830715	5,70237816	alpha-glucosidase
SJAG_03827	76,7924	2,4037	4,99763478	tryptophan permease
SJAG_03828	38,6559	18,67975	1,04921348	glyceraldehyde-3-phosphate dehydrogenase Tdh1
SJAG_03911	18,29925	6,66472	1,45716835	transcription factor Rsv1
SJAG_04152	34,07395	14,22205	1,26053977	NADH dehydrogenase
SJAG_04167	5,043805	0,611357	3,04442551	P-type ATPase
SJAG_04187	399,352	112,76655	1,82432176	hsp104-like protein
SJAG_04301	3156,08	95,5734	5,04538082	invertase
SJAG_04323	66,26155	20,7473	1,67524835	cardiolipin-specific phospholipase
SJAG_04348	36,7969	7,769485	2,24369335	hypothetical protein
SJAG_04373	51,48345	21,83735	1,23731094	hypothetical protein
SJAG_04374	59,85985	20,67045	1,53401887	hypothetical protein
SJAG_04376	1,387495	0,239964	2,53159268	peptidase
SJAG_04458	27,16445	9,036025	1,58795967	NAD binding dehydrogenase
SJAG_04568	9,150215	2,69024	1,76607076	decaprenyl diphosphate synthase subunit Dps1
SJAG_04590	69,95405	23,3712	1,58167577	hypothetical protein

S3 Table. atf1Δ up-regulated genes

SJAG_04662	7,929175	3,68487	1,10555704	hypothetical protein
SJAG_04664	13,42665	4,49326	1,57926494	protein disulfide isomerase
SJAG_04673	55,69455	21,97705	1,34153841	thiamine transporter Thi9
SJAG_04723	35,76975	10,256815	1,80215723	cell agglutination protein mam3
SJAG_04828	47,03065	20,94525	1,16697817	membrane transporter
SJAG_04830	197,9915	74,5486	1,40918533	NiCoT heavy metal ion transporter Nic1
SJAG_04831	55,62585	4,39112	3,66309461	hypothetical protein
SJAG_04833	4,808525	0,5627125	3,0951245	hypothetical protein
SJAG_04866	2,70414	0,3138275	3,10712616	hypothetical protein
SJAG_04927	405,6065	178,4075	1,18490451	inosine-uridine preferring nucleoside hydrolase
SJAG_04950	5,219825	1,71713	1,60400217	tat binding protein 1(TBP-1)-interacting protein
SJAG_04953	8039,635	2814,545	1,51422829	cytosolic thioredoxin Trx1
SJAG_05004	9,29404	3,515715	1,40248773	fungal protein
SJAG_05006	13,08465	2,171105	2,59137393	homeobox transcription factor Phx1
SJAG_05015	162,507	73,83375	1,13814952	NADPH dehydrogenase
SJAG_05201	1,572565	0,420429	1,90318556	hypothetical protein
SJAG_05221	33,45985	8,449645	1,98546834	translation release factor
SJAG_05311	45,2658	22,3167	1,02029774	sphingosine hydroxylase
SJAG_05348	1229,97	514,669	1,25690633	oligosaccharyltransferase subunit Ost4
SJAG_05358	9,34962	2,22779	2,06929449	hypothetical protein
SJAG_05896	27,1796	12,0208	1,17699131	hypothetical protein
SJAG_06097	231,7035	12,44505	4,21863591	hypothetical protein
SJAG_06585	30,83505	5,6095	2,4586271	hypothetical protein
SJAG_06627	5,154365	1,146061	2,16911087	hypothetical protein
SJAG_06641	6,19631	2,061835	1,58748044	hypothetical protein
SJAG_16081	91,40795	29,46455	1,63333941	n/a
SJAG_16103	18,42235	0,5	5,2033852	n/a
SJAG_16119	19,09405	0,5	5,25505124	n/a
SJAG_16129	13,5228	0,5	4,757322	n/a
SJAG_16142	49,0638	19,4437	1,3353562	n/a
SJAG_16303	8,32705	0,5	4,05780549	n/a
SJAG_16445	47,03775	12,46605	1,91581465	n/a
SJAG_16452	1224,585	37,1451	5,0429772	hypothetical protein

S4 Table. atf1Δ down-regulated genes

Gene	ATF1_mean	CONTROL_me	log2FC	description
SJAG_00057	223,016	481,0225	-1,10895716	hexose transporter Ght2
SJAG_00085	16,69245	93,55445	-2,48661056	DUF423 protein
SJAG_00145	13,8455	44,5811	-1,68701506	RNA-binding protein
SJAG_00223	93,0847	929,2205	-3,31940502	hsp9-like protein
SJAG_00254	18,9159	39,04945	-1,04570281	aspartic proteinase sxa1
SJAG_00372	149,103	526,95	-1,82135679	plasma membrane proteolipid Pmp3
SJAG_00501	23,31405	95,9914	-2,04170551	ribulose phosphate 3-epimerase
SJAG_00625	101,89775	214,6395	-1,0747934	hypothetical protein
SJAG_00635	8,483495	25,35125	-1,57932624	ornithine carbamoyltransferase Arg3
SJAG_00668	11,3639	104,869	-3,20605832	superoxide dismutase Sod1
SJAG_00699	70,76145	145,7685	-1,04264348	tspO/peripheral benzodiazepine receptor
SJAG_00709	0,483755	1,94908	-2,01044483	hypothetical protein
SJAG_00789	16,67275	64,51565	-1,95215709	hypothetical protein
SJAG_00812	82,98055	187,0795	-1,17280635	phosphatidyl-N-methylethanolamine N-methyltransferase
SJAG_00890	19,92625	75,0591	-1,91335676	mannose-1-phosphate guanyltransferase
SJAG_00926	28,0165	62,37485	-1,1546877	transcription factor
SJAG_00970	19,0124	79,06055	-2,05601733	actin cortical patch component Lsb4
SJAG_00979	0,4138285	2,79279	-2,75460219	transcription factor atf31
SJAG_00980	0,258785	1,42571	-2,46185466	ATP-dependent DNA helicase Rdh54
SJAG_00981	0,652187	53,25545	-6,35149968	fungal cellulose binding domain-containing protein
SJAG_01017	10,16585	50,22795	-2,30475955	endo-1,3-beta-glucanase Eng2
SJAG_01057	13,4347	50,34585	-1,90590876	dihydroceramide delta-4 desaturase
SJAG_01066	14,25145	28,9241	-1,02116336	hypothetical protein
SJAG_01077	7,90111	17,50955	-1,14801475	cytochrome c oxidase subunit V
SJAG_01089	201,241	433,2365	-1,10623053	UTP-glucose-1-phosphate uridylyltransferase
SJAG_01154	0,9317715	1,903405	-1,03053446	phosphoprotein phosphatase
SJAG_01171	11,18231	33,86205	-1,59845107	glucan 1,3-beta-glucosidase
SJAG_01174	18,0904	49,8082	-1,46115897	Sad1 interacting factor 3
SJAG_01227	21,9884	63,47415	-1,52942654	glycosylceramide biosynthesis protein
SJAG_01262	7,85122	18,19225	-1,21233523	endonuclease Uve1
SJAG_01432	16,8482	46,4439	-1,46289466	hydroxyacid dehydrogenase
SJAG_01493	21,77135	89,5284	-2,03991453	copper transporter complex subunit Ctr5

S4 Table. atf1Δ down-regulated genes

SJAG_01725	10,944945	57,46855	-2,39250794	transcription factor Atf21
SJAG_01757	0,08403505	1,14554	-3,76889284	hypothetical protein
SJAG_01815	10,71115	45,781	-2,09558845	hypothetical protein
SJAG_01904	84,5536	211,904	-1,32547273	hypothetical protein
SJAG_01905	0,939823	10,483995	-3,47965569	progesterone binding protein
SJAG_01965	29,7269	117,3225	-1,98063879	hypothetical protein
SJAG_01968	146,617	426,0035	-1,53881289	pepsin A
SJAG_01982	19,79725	62,29695	-1,65386149	hypothetical protein
SJAG_01985	31,7183	75,83865	-1,25761783	hypothetical protein
SJAG_02016	20,90685	48,03675	-1,20016284	apoptosis-inducing factor Aif1
SJAG_02040	39,53965	107,375	-1,44128613	tubulin specific chaperone cofactor B
SJAG_02150	58,4723	159,739	-1,44989134	amino acid permease inda1
SJAG_02154	6,11194	37,79945	-2,62866296	GFO/IDH/MocA family oxidoreductase
SJAG_02191	67,21825	200,6245	-1,57757291	GFO/IDH/MocA family oxidoreductase
SJAG_02301	44,35205	89,6165	-1,01476359	ER associated protein disulfide isomerase Pdi2
SJAG_02442	11,63375	32,49385	-1,48185048	hypothetical protein
SJAG_02646	7,89437	20,0922	-1,3477395	cytochrome c1 Cyt1
SJAG_02696	9,059455	28,42915	-1,6498748	glucose-6-phosphate 1-dehydrogenase
SJAG_02697	361,251	2609,39	-2,8526391	ubiquitinated histone-like protein Uhp1
SJAG_02744	27,8429	85,72525	-1,62241072	cytochrome c
SJAG_02799	18,53065	40,6513	-1,133388	glucan 1,4-alpha-glucosidase
SJAG_02834	0,2257115	10,446155	-5,53234828	siderophore iron transporter 1
SJAG_02958	0,297207	1,1395535	-1,93892866	hexose transporter Ght5
SJAG_02983	0,5	1,342175	-1,42457279	hypothetical protein
SJAG_02987	384,3105	827,8625	-1,10711878	hypothetical protein
SJAG_03013	2,75083	7,06544	-1,36091242	chitin deacetylase Cda1
SJAG_03049	366,742	2338,635	-2,67282931	fungal protein
SJAG_03063	6,24407	160,5175	-4,68410007	dienelactone hydrolase
SJAG_03178	232,842	547,0645	-1,23235962	hypothetical protein
SJAG_03202	3,71334	10,3474	-1,47847898	hypothetical protein
SJAG_03266	355,161	874,8685	-1,30059302	NADP-specific glutamate dehydrogenase Gdh1
SJAG_03293	64,11735	281,5225	-2,13446353	succinate-semialdehyde dehydrogenase
SJAG_03363	14,1678	37,8714	-1,418493	leptomycin efflux transporter Pmd1

S4 Table. atf1Δ down-regulated genes

SJAG_03434	51,9867	159,035	-1,61312982	4-aminobutyrate aminotransferase
SJAG_03497	7,205865	14,45005	-1,00383096	ATP-binding cassette-type vacuolar membrane transporter Hmt1
SJAG_03784	457,4635	917,289	-1,0037197	hypothetical protein
SJAG_03794	21,30585	52,5063	-1,30124093	DNAJ domain-containing protein Psi1
SJAG_03815	30,0942	82,1334	-1,44848356	hsp16-like protein
SJAG_04031	0,933131	1,88392	-1,01358617	ferrichrome synthetase Sib1
SJAG_04043	0,40353	16,41645	-5,34632244	hypothetical protein
SJAG_04247	10,14334	29,0013	-1,51558479	hypothetical protein
SJAG_04269	0,8054355	1,878215	-1,22152125	hypothetical protein
SJAG_04297	1,0731775	2,202005	-1,03692903	sulfonate dioxygenase
SJAG_04375	73,8523	156,9915	-1,08797169	septin Spn3
SJAG_04430	13,7788	70,6924	-2,35910487	hypothetical protein
SJAG_04607	11,54383	24,6897	-1,09678735	CCAAT-binding factor complex subunit Php4
SJAG_04608	12,31475	53,01955	-2,10613709	flavin dependent monooxygenase
SJAG_04625	1,90336	4,53031	-1,25106132	DUF1761 family protein
SJAG_04637	17,13685	92,28685	-2,42902315	general amino acid permease GAP1
SJAG_04675	15,9272	177,694	-3,4798304	iron permease Fip1
SJAG_04743	5,903495	168,974	-4,83908815	ferric reductase transmembrane component
SJAG_04751	5,59802	13,15665	-1,23280364	ELLA family acetyltransferase
SJAG_04777	5,95359	12,8742	-1,11265101	STE/STE11 protein kinase
SJAG_04867	12,4708	25,47315	-1,03042336	ferrous iron transporter Pcl1
SJAG_04868	1,302775	2,82928	-1,11884702	chitin synthase I
SJAG_04944	34,83685	89,6238	-1,36326772	coproporphyrinogen III oxidase
SJAG_05005	6,91778	13,89165	-1,00583693	fungal protein
SJAG_05021	57,8696	171,5655	-1,56788189	RNA-binding protein Vip1
SJAG_05182	8,628025	17,9432	-1,05633494	allantoate permease
SJAG_05208	56,10865	113,516	-1,01660055	splicing factor 3B
SJAG_05213	11,95025	23,9631	-1,00377376	ATP-binding cassette transporter abc1
SJAG_05305	9,796965	53,44455	-2,44763605	membrane protein complex assembly protein
SJAG_05558	44,85575	91,0148	-1,02080823	fungal protein
SJAG_05889	12,9199	29,58455	-1,19524905	hypothetical protein
SJAG_06002	1,79372	9,252875	-2,366947	hypothetical protein
SJAG_16057	0,5	8,91508	-4,15624774	n/a

S4 Table. atf1Δ down-regulated genes

SJAG_16075	22,255265	45,91295	-1,04475445	n/a
SJAG_16118	0,5	31,54525	-5,97935088	n/a
SJAG_16122	0,5	20,83475	-5,38091988	n/a
SJAG_16183	17,3323	38,0743	-1,1353544	n/a

S5 Table. Common up-regulated genes in sty1Δ and atf1Δ cells

Gene	ATF1_mean	STY1_mean	CONTROL_me	log2FC_ATF1	log2FC_STY1	Description
SJAG_00006	3,52446	2,828265	1,0102715	1,80265918	1,48517425	hypothetical protein
SJAG_00084	479,4945	366,671	166,756	1,5237756	1,1367475	adenylyl-sulfate kinase
SJAG_00110	10,45211	7,22275	2,445735	2,09545421	1,56228014	But2 family protein
SJAG_00124	23,6943	1,66348	0,571147	5,37453412	1,54227051	transcriptional regulator NRG1
SJAG_00179	127,9507	382,0535	20,78725	2,62181722	4,20000386	glutathione S-transferase Gst2
SJAG_00258	2,35646	2,58856	1,168465	1,01200667	1,14753524	hypothetical protein
SJAG_00780	7,74405	8,07228	3,74854	1,04675947	1,10664742	hypothetical protein
SJAG_00927	3,357835	4,638925	1,62873	1,04378388	1,51004306	hypothetical protein
SJAG_01239	208,762	53,99655	25,8489	3,01368434	1,06276434	protein phosphatase Fmp31
SJAG_01552	1,376025	1,30329	0,262511	2,3900569	2,31170836	hypothetical protein
SJAG_01690	15,0661	25,12765	2,77317	2,44169805	3,17966779	NADP-dependent L-serine/L-allo-threonine dehydrogenase ydfG
SJAG_01986	126,09425	282,2025	31,3656	2,00724742	3,1694757	alcohol dehydrogenase
SJAG_02106	22,11515	32,4933	9,72536	1,18521147	1,74031871	hypothetical protein
SJAG_02125	1,5768	1,43034	0,3757585	2,06912204	1,92848048	urea transporter
SJAG_02788	10,9714	8,671825	3,759075	1,54529803	1,20595794	fungus protein
SJAG_02955	12,6681	9,830835	2,923165	2,11559699	1,74978269	general amino acid permease AGP2
SJAG_03643	55,77625	39,9933	18,15125	1,61958204	1,13968942	arrestin Aly1
SJAG_03820	3,693395	1,533005	0,6743025	2,45347971	1,18489455	hexose transporter Ght8
SJAG_03822	1,61908	2,992785	0,3968775	2,02840859	2,91472296	alcohol dehydrogenase Adh4
SJAG_04376	1,387495	1,356375	0,239964	2,53159268	2,49886621	peptidase
SJAG_04833	4,808525	1,768965	0,5627125	3,0951245	1,65243559	hypothetical protein
SJAG_05015	162,507	173,3225	73,83375	1,13814952	1,23110661	NADPH dehydrogenase
SJAG_06097	231,7035	95,57135	12,44505	4,21863591	2,94100617	hypothetical protein
SJAG_06627	5,154365	3,01731	1,146061	2,16911087	1,39657909	hypothetical protein
SJAG_16103	18,42235	13,7006	0,5	5,2033852	4,77616717	n/a
SJAG_16119	19,09405	7,6375	0,5	5,25505124	3,93310047	n/a
SJAG_16129	13,5228	7,5881	0,5	4,757322	3,92373869	n/a
SJAG_16303	8,32705	10,0963	0,5	4,05780549	4,33575478	n/a
SJAG_16445	47,03775	26,1039	12,46605	1,91581465	1,06626096	n/a

S6 Table. Common down-regulated genes in sty1Δ and atf1Δ cells

Gene	ATF1_mean	STY1_mean	CONTROL_me	log2FC_ATF1	log2FC_STY1	Description
SJAG_00085	16,69245	33,5832	93,55445	-2,48661056	-1,47806657	DUF423 protein
SJAG_00145	13,8455	15,8531	44,5811	-1,68701506	-1,49166723	RNA-binding protein
SJAG_00223	93,0847	48,6741	929,2205	-3,31940502	-4,25479477	hsp9-like protein
SJAG_00372	149,103	156,1285	526,95	-1,82135679	-1,75493216	plasma membrane proteolipid Pmp3
SJAG_00625	101,89775	76,95695	214,6395	-1,0747934	-1,47979207	hypothetical protein
SJAG_00635	8,483495	7,916765	25,35125	-1,57932624	-1,67907395	ornithine carbamoyltransferase Arg3
SJAG_00699	70,76145	62,72575	145,7685	-1,04264348	-1,21654927	tspO/peripheral benzodiazepine receptor
SJAG_00709	0,483755	0,725534	1,94908	-2,01044483	-1,42567818	hypothetical protein
SJAG_00789	16,67275	4,04648	64,51565	-1,95215709	-3,9949098	hypothetical protein
SJAG_00812	82,98055	90,649	187,0795	-1,17280635	-1,04528847	phosphatidyl-N-methylethanolamine N-methyltransferase
SJAG_00979	0,4138285	0,559284	2,79279	-2,75460219	-2,32005413	transcription factor atf31
SJAG_00980	0,258785	0,481918	1,42571	-2,46185466	-1,56482096	ATP-dependent DNA helicase Rdh54
SJAG_00981	0,652187	14,18285	53,25545	-6,35149968	-1,90878171	fungal cellulose binding domain-containing protein
SJAG_01432	16,8482	23,1352	46,4439	-1,46289466	-1,00539955	hydroxyacid dehydrogenase
SJAG_01725	10,944945	14,7266	57,46855	-2,39250794	-1,96434826	transcription factor Atf21
SJAG_01757	0,08403505	0,463756	1,14554	-3,76889284	-1,30458998	hypothetical protein
SJAG_01815	10,7115	10,44543	45,781	-2,09558845	-2,13187709	hypothetical protein
SJAG_01905	0,939823	2,58805	10,483995	-3,47965569	-2,01825118	progesterone binding protein
SJAG_01968	146,617	128,5035	426,0035	-1,53881289	-1,72905763	pepsin A
SJAG_02442	11,63375	11,92445	32,49385	-1,48185048	-1,44624396	hypothetical protein
SJAG_02744	27,8429	15,508	85,72525	-1,62241072	-2,46670757	cytochrome c
SJAG_02983	0,5	0,5	1,342175	-1,42457279	-1,42457279	hypothetical protein
SJAG_03063	6,24407	47,9229	160,5175	-4,68410007	-1,74394347	dienelactone hydrolase
SJAG_03794	21,30585	26,2432	52,5063	-1,30124093	-1,00054689	DNAJ domain-containing protein Psi1
SJAG_04043	0,40353	1,145435	16,41645	-5,34632244	-3,84117469	hypothetical protein
SJAG_04297	1,0731775	0,2512055	2,202005	-1,03692903	-3,13187779	sulfonate dioxygenase
SJAG_04375	73,8523	45,27445	156,9915	-1,08797169	-1,79391743	septin Spn3
SJAG_04430	13,7788	33,1786	70,6924	-2,35910487	-1,09130211	hypothetical protein
SJAG_04625	1,90336	0,9118215	4,53031	-1,25106132	-2,31278644	DUF1761 family protein
SJAG_04868	1,302775	1,2909	2,82928	-1,11884702	-1,13205771	chitin synthase I
SJAG_05005	6,91778	3,9484	13,89165	-1,00583693	-1,81487791	fungal protein
SJAG_05305	9,796965	14,42907	53,44455	-2,44763605	-1,88906452	membrane protein complex assembly protein

S6 Table. Common down-regulated genes in sty1Δ and atf1Δ cells

SJAG_05558	44,85575	40,4894	91,0148	-1,02080823	-1,1685569	fungal protein
SJAG_06002	1,79372	2,33124	9,252875	-2,366947	-1,98880416	hypothetical protein
SJAG_16057	0,5	0,5	8,91508	-4,15624774	-4,15624774	n/a
SJAG_16122	0,5	0,5	20,83475	-5,38091988	-5,38091988	n/a
SJAG_16183	17,3323	11,58695	38,0743	-1,1353544	-1,71631665	n/a

S7 Table. Common genes up-regulated in *sty1Δ* cells and down-regulated in *atf1Δ* cells

Gene

SJAG_02834

SJAG_04269

SJAG_04743

SJAG_16075

SJAG_16118

S8 Table. Common genes up-regulated in *sty1Δ* cells and down-regulated in *atf1Δ* cells

Gene

SJAG_00097
SJAG_00099
SJAG_00788
SJAG_01490
SJAG_02338
SJAG_02569
SJAG_02950
SJAG_03818
SJAG_04458
SJAG_04568
SJAG_04662
SJAG_04673
SJAG_05896
SJAG_16142